

# Exact holographic RG flows and the $A_1 \times A_1$ Toda chain

---

Irina Ya. Aref'eva,<sup>a</sup> Anastasia A. Golubtsova<sup>b,c</sup> and Giuseppe Policastro<sup>d</sup>

<sup>a</sup>*Steklov Mathematical Institute, Russian Academy of Sciences,  
Gubkina str. 8, 119991, Moscow, Russia*

<sup>b</sup>*Bogoliubov Laboratory of Theoretical Physics, JINR,  
141980 Dubna, Moscow region, Russia*

<sup>c</sup>*Dubna State University,  
Universitetskaya str. 19, Dubna, 141980, Russia*

<sup>d</sup>*Laboratoire de Physique Théorique de l'École Normale Supérieure,  
PSL University, CNRS, Sorbonne Universités, UPMC Univ. Paris 06,  
24 rue Lhomond, 75231 Paris Cedex 05, France*

*E-mail:* [arefeva@mi.ras.ru](mailto:arefeva@mi.ras.ru), [golubtsova@theor.jinr.ru](mailto:golubtsova@theor.jinr.ru),  
[policast@lpt.ens.fr](mailto:policast@lpt.ens.fr)

ABSTRACT: We construct analytic solutions of Einstein gravity coupled to a dilaton field with a potential given by a sum of two exponentials, by rewriting the equations of motion in terms of an integrable Toda chain. Such solutions can be interpreted as domain walls interpolating between different asymptotics, and as such they can have interesting applications in holography. In some cases we can find flows that start from an AdS fixed point. We also find analytic black brane solutions at finite temperature. We discuss the properties of the solutions and the interpretation in terms of RG flow.

---

## Contents

<b>1</b>	<b>Introduction</b>	<b>2</b>
<b>2</b>	<b>The setup</b>	<b>4</b>
2.1	The holographic gravity model	5
2.2	Integration of the mechanical model	7
2.3	The exact solutions of the holographic model	9
<b>3</b>	<b>Vacuum solutions</b>	<b>10</b>
3.1	The metric and the dilaton	10
3.2	Asymptotics of the metric and the dilaton	12
3.2.1	Special case, solutions with $u_{01} = u_{02}$	15
<b>4</b>	<b>Non-vacuum solutions</b>	<b>17</b>
4.1	Black branes	17
4.1.1	Black brane in the IR-limit	18
4.1.2	Black brane in the UV-limit	19
4.2	The asymptotics of the metric and the dilaton	20
4.3	The special case $u_{01} = u_{02}$	22
<b>5</b>	<b>Holographic RG flows</b>	<b>24</b>
5.1	The domain-wall coordinates	25
5.2	RG flow at zero-temperature	26
5.3	Non-vacuum RG flow	31
5.4	The running coupling $\lambda = e^\phi$ on the energy scale. Vacuum flow	35
5.5	The running coupling $\lambda = e^\phi$ on the energy scale. Non-vacuum flow	38
5.5.1	Three branch solutions with $u_{01} \neq u_{02}$	38
5.5.2	Special case $u_{01} = u_{02}$	42
<b>6</b>	<b>Conclusion and Discussion</b>	<b>42</b>
<b>A</b>	<b>The curvature invariants of the background</b>	<b>44</b>
A.1	The scalar curvature of the vacuum solutions.	45
A.2	The scalar curvature of the non-vacuum solutions.	48
A.3	The Kretschmann scalar for the solution with $u > u_{01}$	50
<b>B</b>	<b>The scalar field</b>	<b>51</b>
<b>C</b>	<b>Details of the non-vacuum RG</b>	<b>52</b>

---

## 1 Introduction

The notion of the renormalization group has dominated our thinking about quantum field theories and statistical systems since its elaboration by K. Wilson. It has been a paradigm-changing idea, providing a unified and systematic picture to understand the dynamics of systems with many degrees of freedoms. Quantum field theories are now not seen as isolated items, but as classes connected by the RG flow. The method is very powerful, however in practice one can usually only determine the structure of the flow in a perturbative expansion around a fixed point that is weakly coupled. Luckily there are many interesting theories for which the program can be implemented, including of course Yang-Mills and QCD that are asymptotically free, the Wilson-Fisher fixed point of  $\lambda\phi^4$  in dimension  $4 - \epsilon$ , etc, but strongly-coupled examples are few.

The holographic correspondence gives a description of a class of strongly-coupled field theories in terms of a dual weakly-coupled gravitational description. The RG flow in this description is geometrized, and corresponds to a gravitational solution with particular asymptotic properties; the holographic direction corresponds to the energy scale, and so the Hamiltonian evolution in this direction can be put in correspondence with the evolution of the system under the change of the RG scale [1]. These solutions are often described as “domain wall” solutions, as they interpolate between two asymptotic regions, each of them being a solution on its own and corresponding to a given theory.

This aspect of the holographic correspondence has been intensely explored, but some issues have so far eluded a complete resolution; for instance, the precise relation between the holographic and the Wilsonian scheme [2, 3], and the fact that Einstein equations are second order while RG equations are first-order; even though the equations can be cast in first-order form using the Hamilton-Jacobi formalism, there seems still to be a mismatch in that the couplings of the field theory are promoted to fluctuating fields in the gravity description; recently an attempt to solve this problem has been made [4] with the notion of a “quantum RG flow”, that arises from the classical one after integrating out the double-trace operators. This flow may be more complex than the one typically arising in QFT, and these possibilities have only been considered in the last few years [5].

The matching of RG equations with the gravity equations has been precisely formulated only for the solutions that have Poincaré invariant at the boundary, and correspond to the vacuum of the dual field theory. In these cases, one can show that the equations of motion can be expressed in terms of a superpotential, which is determined by the scalar potential (up to the choice of some integration constants), and is in one-to-one correspondence with the beta function of the dual theory. But it is not yet known how to extend this procedure to non-Poincaré invariant states, in particular finite temperature/density.

In this paper we will not be concerned with these conceptual issues. Rather, in the spirit of “bottom-up” holography, we remark that there are some relatively simple models of gravity coupled to a scalar field, that allow for interesting examples of RG flows that can be found analytically. This is due to the fact that the Einstein equations, with the Ansatz that corresponds to domain-walls solutions, reduce to dynamical equations that are completely integrable (they can be reduced to the equations of a Toda chain). It is

remarkable that such analytic domain-wall solutions can be found not only for the vacuum but also at finite temperature. The Toda equations arise when the potential is a sum of exponentials, when the coefficients in the exponent satisfy certain relations. The case of a single exponential term had been solved in [6]. The Chamblin-Reall black brane solution has found applications to the study of the dynamics of a non-conformal strongly coupled plasma in the hydro regime and beyond [7, 8]. However the single exponential case has some limitations: the potential is monotonous, so it does not have a minimum but only run-away solutions; the RG flow in this case does not start from a UV fixed point, and in fact the dual theory is not well-behaved in the UV. Moreover, the single exponential has a definite sign. This precludes the possibility of studying cases in which the potential changes sign along the solution. The general analysis of RG flow with a single scalar, performed in [5], only deals with potentials that are definite negative; the general case of a potential with zeros is less explored.

In this paper we consider the next simplest case, with a sum of two exponentials. Integrability leaves one of the two exponents unfixed, so we have one free parameter, like in the case of a single exponential. This case already allows to overcome the limitations just mentioned. We will leave the consideration of more complicated potentials for future investigations. Qualitatively, the properties of the potential is that it has a minimum with  $V_{min} < 0$ , it goes from being negative and vanishing at  $\phi \rightarrow -\infty$  to positive and diverging at  $\phi \rightarrow +\infty$ .

It turns out that for our choice of potential, the integrable Toda chain is associated to the Lie algebra is  $A_1 \times A_1$  [9, 10], so it is a particularly simple case and the solutions can be given explicitly in terms of elementary functions.

The solutions we find depend on a certain number of parameters. One parameter distinguishes between vacuum and nonvacuum solutions. The vacuum solutions are Poincaré invariant. Turning on the parameter gives a deformation to non-vacuum solutions, in which Poincaré symmetry is broken, and horizons can be formed. Other parameters determine the type of solutions; there are 4 general classes of vacuum solutions – depending on the type of functions that appear, we will call them the sinh-class, sin-classe, linear class and cosh-class of solutions (see eqs.(2.33)). We will consider mainly the sinh-class. Two other parameters determine the position of singularities, whose presence requires to split the domain on the radial variable in three regions; correspondingly we have "left", "middle" and "right" solutions; one more constant is the "energy" of the solutions (more exactly the energy in the associated Toda chain description). In the left and middle solutions the dilaton interpolates between  $+\infty$  and  $-\infty$ , whereas the right solution is bouncing: the dilaton starts at  $-\infty$ , goes to a maximal value and then goes back to  $-\infty$ . It should be noted that the singularities are not just coordinate singularities; the scalar curvature usually diverges at the end points of the branches, except for the right end of the middle branch.

It is interesting that, in spite of the fact that the dilaton has similar behaviour in the left and middle solutions, the scale factor, that characterizes the metric, has rather different behaviour on these solutions, namely, on the left solution when dilaton varies from  $-\infty$  to a special value  $\phi_s$ , the scale factor increases, but after dilaton passes a special value  $\phi_s$ , the scale factor starts to decrease down to zero. This non-monotonic behavior of

the scale factor precludes the possibility of a holographic interpretation of this branch of solutions. For the middle solution, when dilaton increases from  $-\infty$  to  $\infty$ , the scale factor decreases from large positive values to zero. This behaviour corresponds to the running of a coupling in an asymptotically free theory, so it is of interest from the point of view of possible applications in QCD. In the right solution the scale factor is increasing from zero to infinity, but the dilaton bounces back after reaching a maximal value  $\phi_{max}$ , as already mentioned. These behaviours are illustrated in Figs. (23,24).

There is also a special case when the points of singularities coincide, and the middle solutions disappears. The singularities are cancelled in this case and the solution has a smooth AdS limit. In this case the dilaton runs from a constant in the UV to  $-\infty$  in the IR.

When we turn to non-vacuum solutions, the deformation can give solutions with a horizon or without. For the cases having horizons, the parameter characterizing the deformation is related to the temperature. It happens that the black brane solutions can be constructed only from those vacuum solutions which are defined for  $u \rightarrow \pm\infty$ , so only in the left or right branch. In particular, for the solutions defined for  $u \rightarrow +\infty$  we change the scaling properties of these solutions in the IR regime varying the temperature, meanwhile the UV behavior does not change. We observe that there is a special value of the scale factor  $A_0$ , such that increasing the scale factor from this value the dilaton decreases for all temperatures, providing for a corresponding (hypothetic) dual gauge theory the asymptotic freedom. For scalar factor less then  $A_0$ , there are two different regime: in one case the dilaton goes to zero when  $A$  goes to zero, like in the bouncing solutions at zero temperature; however in the other regime the dilaton blows up providing the IR confinement for the dual theory. This behaviour is illustrated in Figs. (28, 29).

The interpretation of the solutions in terms of RG flows is clarified by using the first order variables  $X, Y$  [11] that have a direct relation to the superpotential and the beta function, when a dual theory interpretation is possible. We discuss how our solutions describe flows between different attractor points in the phase space, i.e. the  $(\phi, X)$  plane, but in order to recover all possible flows we also have to include other classes of solutions, namely the linear and *cosh* solutions. This is illustrated in Figs. 15 and 16. In Fig. 17 we show the map of possible flows at non-zero temperature.

The paper is organized as follows. In Sect. 2 we describe the holographic gravity model, the ansatz for the metric and the dilaton that leads to a special mechanical model, that can be explicitly integrated. In Sect. 3 we describe metric and dilaton for vacuum solutions. In Sect. 4 we study non-vacuum solutions and in Sect. 5 we study the renormalization group flows corresponding to the constructed solutions. In the Appendix, we collect information about curvature invariants for our background in Sect. A, some formula about the dilaton field in Sect. B and more details about the RG for non-vacuum case in Sect. C.

## 2 The setup

We consider a holographic model with gravity coupled to a dilaton field, and the dilaton potential is taken as a sum of two exponential functions. As explained in the introduc-

tion, the choice of the dilaton potential is motivated by studies of models with only one exponential function in the potential [7],[11].

## 2.1 The holographic gravity model

The holographic model is governed by an action of the form

$$\mathcal{A} = \frac{1}{16\pi G_5} \int d^5x \sqrt{|g|} \left( R - \frac{4}{3} (\partial\phi)^2 - V(\phi) \right) + G.H., \quad (2.1)$$

with the dilaton potential

$$V(\phi) = C_1 e^{2k_1\phi} + C_2 e^{2k_2\phi}, \quad (2.2)$$

where  $C_i, k_i$  with  $i = 1, 2$  are constants. We choose the constants as follows

$$C_1 < 0, \quad C_2 > 0. \quad (2.3)$$

In this case the potential has a minimum and regions of positive and negative sign, as shown in Fig. 1.

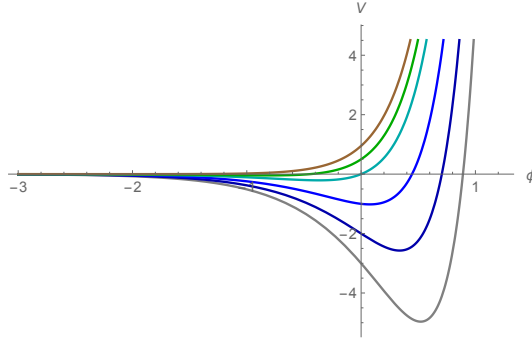


**Figure 1.** The behaviour of the potential  $V(\phi)$  for  $C_1 < 0, C_2 > 0$ .

The model (2.1)-(2.2) is defined on a 5-dim manifold  $M$  equipped with the metric

$$ds^2 = -e^{2A(u)} dt^2 + e^{2B(u)} \sum_{i=1}^3 dy_i^2 + e^{2C(u)} du^2, \quad (2.4)$$

where  $A = A(u)$ ,  $B = B(u)$  and  $C = C(u)$  are some smooth functions. We make an ansatz in which these functions, as well as the dilaton, depend only on the  $u$ -coordinate.

The equations of motion which follow from the action (2.1) read

$$R_{MN} - \frac{1}{2} g_{MN} R = \frac{4}{3} \left( \partial_M \phi \partial_N \phi - \frac{1}{2} g_{MN} \partial_k \phi \partial^k \phi \right) - \frac{1}{2} g_{MN} V(\phi). \quad (2.5)$$

The equation for the scalar field is

$$\square\phi = \frac{3}{8} \frac{\partial V}{\partial \phi}. \quad (2.6)$$

Taking into account the relations (A.2)-(A.6), (B.1), the Lagrangian can be reduced to the following form, up to total derivative terms :

$$L = \frac{1}{2} \left[ -e^{A+3B-C} (6\dot{A}\dot{B} + 6\dot{B}^2) + \frac{4}{3} \dot{\phi}^2 e^{A+3B-C} + e^{A+3B+C} V(\phi) \right], \quad (2.7)$$

where we denote  $\dot{\phantom{x}} \equiv \frac{d}{du}$ . For convenience we redefine the functions as

$$A(u) = x^1(u), \quad B(u) = x^2(u), \quad \phi(u) = x^3(u), \quad C(u) = x(u), \quad (2.8)$$

introduce a new variable  $x_0$

$$x_0 = x^1 + 3x^2 \quad (2.9)$$

and the so-called lapse function

$$\mathcal{N} = e^{x-x_0}. \quad (2.10)$$

In what follows we use the harmonic gauge, i.e.

$$\mathcal{N} = 1, \quad \text{or} \quad x = x_0. \quad (2.11)$$

The Lagrangian (2.7) with the help of (2.8)-(2.11) can be taken to the following form (see [17] and refs. therein)

$$L = \frac{1}{2} G_{ij} \dot{x}^i \dot{x}^j - V(x), \quad (2.12)$$

$$V = -\frac{1}{2} \sum_{s=1}^2 C_s e^{2(x^1+3x^2+k_s x^3)}, \quad (2.13)$$

where the minisupermetric  $G_{ij}$  on the target space  $\mathcal{M}$  reads

$$(G_{ij}) = \begin{pmatrix} 0 & -3 & 0 \\ -3 & -6 & 0 \\ 0 & 0 & \frac{4}{3} \end{pmatrix}, \quad (G^{ij}) = \begin{pmatrix} \frac{2}{3} & -\frac{1}{3} & 0 \\ -\frac{1}{3} & 0 & 0 \\ 0 & 0 & \frac{3}{4} \end{pmatrix}, \quad i, j = 1, 2, 3. \quad (2.14)$$

The corresponding energy constraint is given by

$$E = \frac{1}{2} G_{ij} \dot{x}^i \dot{x}^j + V = 0. \quad (2.15)$$

However, the system (2.12)-(2.15) is still difficult to work with, because of the degrees of freedom are coupled in the potential. The idea of the next section is to separate the equations of motion rotating the system.

## 2.2 Integration of the mechanical model

To perform the following calculations it is useful to present the mechanical Lagrangian (2.12) in the form

$$L = \frac{1}{2} \langle \dot{x}, \dot{x} \rangle + \frac{C_1}{2} e^{\langle V, x \rangle} + \frac{C_2}{2} e^{\langle W, x \rangle}, \quad (2.16)$$

where  $V$  and  $W$  are some vectors on the target space (we suppose that the original basis is  $(e_1, e_2, e_3)$ ), the brackets denote a scalar product on the target space  $\mathcal{M}$  defined by the metric (2.14).

Then the components of  $V$  and  $W$  are defined by

$$V^1 = -\frac{2}{3}, \quad V^2 = -\frac{2}{3}, \quad V^3 = \frac{3}{2}k_1, \quad (2.17)$$

$$W^1 = -\frac{2}{3}, \quad W^2 = -\frac{2}{3}, \quad W^3 = \frac{3}{2}k_2. \quad (2.18)$$

The method we will use applies generally to systems with interactions of the form (2.16), with arbitrarily many exponentials [15, 16]. It turns out that the system is integrable if the vectors  $V$  and  $W$  can be identified with the root vectors of a Lie algebra (for more details see [9, 10]). The system becomes a Toda chain. In our case, we can see that the scalar products of the vectors are:

$$\langle V, V \rangle = 3 \left( k_1^2 - \frac{16}{9} \right), \quad \langle W, W \rangle = 3 \left( k_2^2 - \frac{16}{9} \right), \quad \langle V, W \rangle = 3 \left( k_1 k_2 - \frac{16}{9} \right). \quad (2.19)$$

These correspond to the roots of a Lie algebra only if  $V$  and  $W$  are orthogonal, in which case we have the  $A_1 \times A_1$  Toda model. The integrability requirement puts a restriction on the dilaton couplings:

$$\langle V, W \rangle = 0, \quad k_1 k_2 = \frac{16}{9}. \quad (2.20)$$

We also suppose that  $V$  is a timelike vector and  $W$  is a spacelike one (notice that the symmetry between  $k_1$  and  $k_2$  is broken by the choice of the signs of the coefficients in the potential). We rename

$$k_1 = k, \quad k_2 = \frac{16}{9k}, \quad (2.21)$$

and we have the condition

$$0 < k < 4/3. \quad (2.22)$$

We can find a basis of orthonormal vectors with respect to the metric  $G_{MN}$ :

$$\langle e'_i, e'_j \rangle = \eta_{ij}, \quad \text{with} \quad (\eta_{ij}) = \text{diag}(-1, 1, 1); \quad (2.23)$$

one can choose the new basis vectors as follows

$$e'_1 = \frac{V}{\|V\|}, \quad e'_2 = \frac{W}{\|W\|}. \quad (2.24)$$

The new basis is related to the old one by a Lorentz transformation:

$$e'_j = \sum_{i=1}^3 S_j^i e_i, \quad \sum_{k,l=1}^n G_{kl} S_i^k S_j^l = \eta_{ij}, \quad (2.25)$$

and the coordinates transform as

$$x^i = \sum_{j=1}^3 S_j^i X^j, \quad X^i = \eta_{ii} \langle e'_i, x \rangle. \quad (2.26)$$

The Lagrangian and the energy constraint (2.12)-(2.15) in the new basis take the form

$$L = \frac{1}{2} \sum_{i,j=1}^3 \eta_{ij} \dot{X}^i \dot{X}^j + \frac{C_1}{2} \exp \left[ \eta_{11} |\langle V, V \rangle|^{1/2} X^1 \right] + \frac{C_2}{2} \exp \left[ \eta_{22} |\langle W, W \rangle|^{1/2} X^2 \right], \quad (2.27)$$

$$E_0 = \frac{1}{2} \sum_{i,j=1}^3 \eta_{ij} \dot{X}^i \dot{X}^j - \frac{C_1}{2} \exp \left[ \eta_{11} |\langle V, V \rangle|^{1/2} X^1 \right] - \frac{C_2}{2} \exp \left[ \eta_{22} |\langle W, W \rangle|^{1/2} X^2 \right]. \quad (2.28)$$

From (2.27)-(2.28) we see that mechanical variables are decoupled, so the equations of motion following from the Lagrangian (2.27) are

$$\ddot{X}^s = |\langle R_s, R_s \rangle|^{1/2} \frac{C_s}{2} \exp \left[ \eta_{ss} |\langle R_s, R_s \rangle|^{1/2} X^s \right], \quad s = 1, 2, \quad (2.29)$$

$$\ddot{X}^3 = 0, \quad (2.30)$$

where  $s = 1, 2$  and we introduce a notation for the scalar product

$$\langle R_1, R_1 \rangle = \langle V, V \rangle, \quad \langle R_2, R_2 \rangle = \langle W, W \rangle. \quad (2.31)$$

The eqs. (2.29) with  $s = 1, 2$  are two decoupled Liouville equations. The solution can be given explicitly:

$$X^s = -\eta_{ss} |\langle R_s, R_s \rangle|^{-1/2} \ln F_s^2(u - u_{0s}), \quad (2.32)$$

with the functions

$$F_s(u - u_{0s}) = \begin{cases} \sqrt{\frac{|C_s|}{2|E_s|}} \sinh \left[ \sqrt{\frac{|E_s \langle R_s, R_s \rangle|}{2}} (u - u_{0s}) \right], & \text{if } \eta_{ss} C_s > 0, \quad \eta_{ss} E_s > 0, \\ \sqrt{\frac{|C_s|}{2|E_s|}} \sin \left[ \sqrt{\frac{|E_s \langle R_s, R_s \rangle|}{2}} (u - u_{0s}) \right], & \text{if } \eta_{ss} C_s > 0, \quad \eta_{ss} E_s < 0, \\ \sqrt{\frac{|\langle R_s, R_s \rangle C_s|}{4}} (u - u_{0s}), & \text{if } \eta_{ss} C_s > 0, \quad E_s = 0, \\ \sqrt{\frac{|C_s|}{2|E_s|}} \cosh \left[ \sqrt{\frac{|E_s \langle R_s, R_s \rangle|}{2}} (u - u_{0s}) \right], & \text{if } \eta_{ss} C_s < 0, \quad \eta_{ss} E_s > 0, \end{cases} \quad (2.33)$$

where  $u_{0s}$ ,  $E_s$  are constants of integration,  $s = 1, 2$ . The  $E_s$  are the conserved energies of the two decoupled Liouville modes. In our case, with  $C_1 < 0$  and  $C_2 > 0$ , we have  $\eta_{ss}C_s > 0$ , so the relevant solutions are given by the first three lines. We will analyze in detail the sinh solutions, which are the most interesting from the RG point of view.

The solutions to eq. (2.30) is

$$X^3 = p^3 u + q^3, \quad (2.34)$$

with constants of integration  $p^3$ ,  $q^3$ .

Having solved the system, we can go back to the original variables applying the transformations (2.32) with components

$$S_1^i = \frac{V^i}{|\langle V, V \rangle|^{1/2}}, \quad S_2^i = \frac{W^i}{\langle W, W \rangle^{1/2}}, \quad (2.35)$$

and obtain

$$\exp x^1 = [F_1(u - u_{01})]^{-\frac{2V^1}{\langle V, V \rangle}} [F_2(u - u_{02})]^{-\frac{2W^1}{\langle W, W \rangle}} e^{\alpha^1 u + \beta^1}, \quad (2.36)$$

$$\exp x^2 = [F_1(u - u_{01})]^{-\frac{2V^2}{\langle V, V \rangle}} [F_2(u - u_{02})]^{-\frac{2W^2}{\langle W, W \rangle}} e^{\alpha^2 u + \beta^2}, \quad (2.37)$$

$$\exp x^3 = [F_1(u - u_{01})]^{-\frac{2V^3}{\langle V, V \rangle}} [F_2(u - u_{02})]^{-\frac{2W^3}{\langle W, W \rangle}} e^{\alpha^3 u + \beta^3}. \quad (2.38)$$

with the parameters  $\alpha^i$ ,  $\beta^i$  defined using (2.25)

$$\alpha^i = S_3^i p^3, \quad \beta^i = S_3^i q^3. \quad (2.39)$$

The parameters  $\alpha^i$  satisfy the following conditions

$$\langle \alpha, V \rangle = 0, \quad \langle \alpha, W \rangle = 0 \quad (2.40)$$

which imply

$$\alpha^3 = 0, \quad \alpha^1 = -3\alpha^2. \quad (2.41)$$

The constants  $E_1$ ,  $E_2$  and  $\alpha^i$  are related by the constraint (2.28) which reads

$$E_1 + E_2 + \frac{1}{2} \langle \alpha, \alpha \rangle = E_0. \quad (2.42)$$

### 2.3 The exact solutions of the holographic model

Keeping in mind that the variables  $x^i$  with (2.36)-(2.38) are redefined metric functions  $A$ ,  $B$  and the dilaton  $\phi$  (2.8)-(2.9), and taking the gauge condition  $C = A + 3B$  (2.11) into account, we can write down the metric coefficients of (2.4)

$$e^A = F_1^{\frac{4}{9k^2-16}} F_2^{\frac{9k^2}{4(16-9k^2)}} e^{\alpha^1 u}, \quad (2.43)$$

$$e^B = F_1^{\frac{4}{9k^2-16}} F_2^{\frac{9k^2}{4(16-9k^2)}} e^{\alpha^2 u}, \quad (2.44)$$

$$e^C = F_1^{\frac{16}{9k^2-16}} F_2^{\frac{9k^2}{16-9k^2}} e^{\alpha^3 u}, \quad (2.45)$$

where for simplicity we put  $\beta^i$ ,  $i = 1, 2, 3$ , to zero (without loss of generality, as this corresponds to a rescaling of the coordinates). For the dilaton we have

$$\phi = -\frac{9k}{9k^2 - 16} \ln F_1 + \frac{9k}{9k^2 - 16} \ln F_2, \quad (2.46)$$

moreover the dilaton equation (2.6) requires to take  $E_0 = 0$  in (2.42), so the constraint (2.42) reads

$$E_1 + E_2 + \frac{2(\alpha^1)^2}{3} = 0, \quad (2.47)$$

with  $E_1 < 0$ ,  $E_2 > 0$  and the value of  $E_1$  is bounded as  $|E_1| = E_2 + \frac{2(\alpha^1)^2}{3}$ .

Then the functions  $F_1$  and  $F_2$  in (2.43)-(2.46) are given by

$$F_1 = \sqrt{\left| \frac{C_1}{2E_1} \right|} \sinh(\mu_1 |u - u_{01}|), \quad \mu_1 = \sqrt{\left| \frac{3E_1}{2} \left( k^2 - \frac{16}{9} \right) \right|} \quad (2.48)$$

$$F_2 = \sqrt{\left| \frac{C_2}{2E_2} \right|} \sinh(\mu_2 |u - u_{02}|), \quad \mu_2 = \sqrt{\left| \frac{3E_2}{2} \left( \left( \frac{16}{9} \right)^2 \frac{1}{k^2} - \frac{16}{9} \right) \right|}, \quad (2.49)$$

where  $0 < k < 4/3$ ,  $s = 1, 2$ ,  $C_1$  and  $C_2$  are given by (2.2)-(2.3). The generic form of the metric that solves EOM following from (2.1) reads

$$ds^2 = F_1^{\frac{8}{9k^2-16}} F_2^{\frac{9k^2}{2(16-9k^2)}} \left( -e^{2\alpha^1 u} dt^2 + e^{2\alpha^2 u} d\vec{y}^2 \right) + F_1^{\frac{32}{9k^2-16}} F_2^{\frac{18k^2}{16-9k^2}} du^2, \quad (2.50)$$

where  $\vec{y} = (y_1, y_2, y_3)$ .

The dilaton potential evaluated on the solution becomes

$$V = C_1 e^{2k\phi} + C_2 e^{32\phi/(9k)} = C_1 \left( \frac{F_2}{F_1} \right)^{\frac{18k^2}{9k^2-16}} + C_2 \left( \frac{F_2}{F_1} \right)^{\frac{32}{9k^2-16}}. \quad (2.51)$$

### 3 Vacuum solutions

#### 3.1 The metric and the dilaton

The vacuum solutions are those that preserve Poincaré invariance on the boundary. As can be seen from (2.50), this requires that  $\alpha^1 = \alpha^2 = 0$ , so in this case the two Liouville energies have to be opposite:

$$|E_1| = |E_2|, \quad (3.1)$$

with  $E_1 < 0$ ,  $E_2 > 0$ .

Owing to (3.1) the metric (2.50) takes the form

$$ds^2 = F_1^{\frac{8}{9k^2-16}} F_2^{\frac{9k^2}{2(16-9k^2)}} (-dt^2 + d\vec{y}^2) + F_1^{\frac{32}{9k^2-16}} F_2^{\frac{18k^2}{16-9k^2}} du^2, \quad (3.2)$$

and the dilaton is given by

$$\phi = \frac{9k}{9k^2 - 16} \log \left( \sqrt{\frac{C_2 \sinh(\mu_2 |u_{02} - u|)}{|C_1| \sinh(\mu_1 |u - u_{01}|)}} \right). \quad (3.3)$$

In the vacuum case, the following relation holds:

$$\frac{\mu_2}{\mu_1} = \frac{4}{3k} > 1. \quad (3.4)$$

From the form of the functions  $F_1$  and  $F_2$  given by (2.48)-(2.49) we can see that the solution will have coordinate singularities at the points  $u_{01}, u_{02}$ . We have to consider three coordinate charts. Let us take  $u_{02} < u_{01}$  (for definiteness we consider  $u_{01} > 0$ ). Then the charts are

### 3-branch solution

$$\text{left: } u < u_{02} \quad (3.5)$$

$$\text{middle: } u_{02} < u < u_{01} \quad (3.6)$$

$$\text{right: } u > u_{01} \quad (3.7)$$

The degenerate case with  $u_{01} = u_{02} = u_0$  requires only two charts:

### 2-branch solution

$$\text{left: } u < u_0 \quad (3.8)$$

$$\text{right: } u > u_0. \quad (3.9)$$

The behaviours of the dilaton solutions for  $u_{01} > u_{02}$  are presented in Fig. 2 A. The case  $u_{01} < u_{02}$  corresponds to the reflection of the plot about the vertical axis and shown in Fig. 2 B.

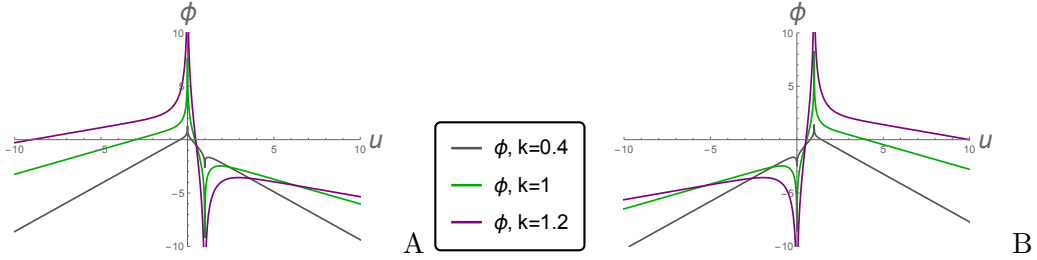


**Figure 2.** The dilaton solutions (3.3) as functions of  $u$ ,  $|E_1| = -|E_2| = -1$ ,  $C_1 = -C_2 = -1$ ,  $k = 0.4, 1, 1.2$ : A) for  $u_{01} = 1$ ,  $u_{02} = 0$ , B) for  $u_{01} = 0$ ,  $u_{02} = 1$ .

In Fig. 3 we plot the solutions for the dilaton  $\phi$  for each choice of the coordinates (3.5)-(3.7).

From Fig. 2 A) and Fig. 3 we see that for  $u \rightarrow u_{01} \pm \epsilon$  the dilaton tends to  $-\infty$ , while for  $u \rightarrow u_{02} \pm \epsilon$  the dilaton asymptotes to  $+\infty$ . It can be verified by direct calculations.

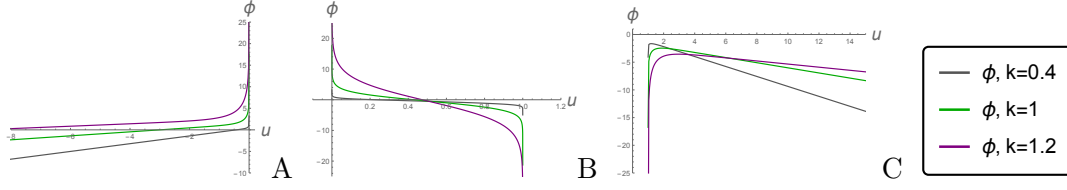


**Figure 3.** The same as in Fig. 2, separately for each type of the solutions: A) the dilaton for  $u < u_{02}$ ,  $u_{02} = 0$  B) the dilaton for  $u_{02} < u < u_{01}$ ,  $u_{01} = 1$ ,  $u_{02} = 0$  C) the dilaton for  $u > u_{01}$ ,  $u_{01} = 1$ . For all  $|E_1| = -|E_2| = -1$ ,  $C_1 = -C_2 = -1$ ,  $k = 0.4, 1, 1.2$ .

### 3.2 Asymptotics of the metric and the dilaton

We present here the asymptotics of the dilaton and the metric near the boundaries of 3 branches solutions with (3.5)-(3.7).

**The left solution** with  $u < u_{02}$

- at  $u \rightarrow -\infty$ :

$$ds^2 \sim z^{2/3} (-dt^2 + dy_1^2 + dy_2^2 + dy_3^2 + dz^2), \quad (3.10)$$

$$\phi \sim \frac{9k}{16-9k^2}(\mu_2 - \mu_1) u \sim \log z \rightarrow -\infty, \quad (3.11)$$

where we use a new coordinate  $z \sim \frac{4+3k}{3\mu_1} e^{\frac{3\mu_1 u}{4+3k}}$ . In Appendix A.1 the scalar curvature of the left solution for both limits is presented. For  $u \rightarrow -\infty$  the scalar curvature of the left solution (A.15) tends to  $+\infty$ .

- at  $u \rightarrow u_{02} - \epsilon$ :

$$ds^2 \sim z^{\frac{18k^2}{64-9k^2}} (-dt^2 + dy_1^2 + dy_2^2 + dy_3^2 + dz^2), \quad (3.12)$$

$$\phi \sim -\frac{36k}{64-9k^2} \log z \rightarrow +\infty, \quad (3.13)$$

with the radial coordinate defined by

$$z \sim \frac{64-9k^2}{4(16-9k^2)} (u - u_{02})^{\frac{64-9k^2}{4(16-9k^2)}}. \quad (3.14)$$

From the relation for the scalar curvature (A.17) with  $u \rightarrow u_{02} - \epsilon$  it can be seen that the solution has a non-removable singularity at the point  $u_{02}$ .

**The middle solution** with  $u_{02} < u < u_{01}$

- at  $u \rightarrow u_{02} + \epsilon$  the asymptotics of the dilaton and the metric are the same as in (3.12),3.13). As in the case of the left solution, one can see from the scalar curvature (A.19) that the middle solution has also a singularity at the point  $u_{02}$ ;

- at  $u \rightarrow u_{01} - \epsilon$  :

$$ds^2 \sim z^{\frac{8}{9k^2-4}} (-dt^2 + dy_1^2 + dy_2^2 + dy_3^2 + dz^2), \quad (3.15)$$

$$\phi \sim \frac{9k}{4-9k^2} \log z \rightarrow -\infty \quad (3.16)$$

where the conformal coordinate is

$$z \sim \frac{16-9k^2}{9k^2-4} (u-u_{01})^{\frac{4-9k^2}{16-9k^2}}. \quad (3.17)$$

Notice that as  $u \rightarrow u_{01}$ , the conformal coordinate  $z \rightarrow 0$  if  $0 < k < 2/3$  and  $z \rightarrow \infty$  if  $2/3 < k < 4/3$ . These asymptotics are the same as for the solutions in a single exponential potential [6]. It is worth noting the scalar curvature of the middle solution (A.20) has a regular behaviour at  $u_{01}$ .

### The right solution with $u > u_{01}$

- at  $u \rightarrow u_{01} + \epsilon$  the asymptotics are as in (3.15)-(3.16).
- at  $u \rightarrow +\infty$  :

$$ds^2 \sim z^{2/3} (-dt^2 + dy_1^2 + dy_2^2 + dy_3^2 + dz^2), \quad (3.18)$$

$$\phi \sim \log z \rightarrow -\infty \quad (3.19)$$

where  $z$  is defined by  $z \sim -\frac{4+3k}{3\mu_1} e^{-\frac{3\mu_1 u}{4+3k}}$ . The asymptotics are the same as in (3.10),(3.11). Even though the dilaton goes to  $-\infty$ , these are different than the asymptotics for a single exponential. The scalar curvature (A.23) goes to  $+\infty$  with  $u \rightarrow +\infty$ .

Now let us turn the discussion to the dilaton potential, that reads

$$V = C_1 e^{2k_1 \phi} + C_2 e^{2k_2 \phi} = C_1 \left( \frac{F_2}{F_1} \right)^{\frac{18k^2}{9k^2-16}} + C_2 \left( \frac{F_2}{F_1} \right)^{\frac{32}{9k^2-16}}. \quad (3.20)$$

In Fig. 4 we present the behaviour of the potential as a function of  $u$  for all dilaton solutions (3.3). In Fig. 5 we plot the dilaton potential on the solutions for  $\phi$ . From Fig. 5 C) one can see that for the solutions defined for  $u > u_{01}$  there is a stop point  $V_s = V(\phi)$  with  $\phi = \phi_s$ , where the potential stops and goes back to zero.

One can find the stop points of the potentials analytically. The stop point  $u_s$  can be calculated as follows. The dilaton should obey

$$\phi' = 0, \quad (3.21)$$

this gives rise to

$$\frac{F_1'}{F_1} = \frac{F_2'}{F_2} \quad (3.22)$$

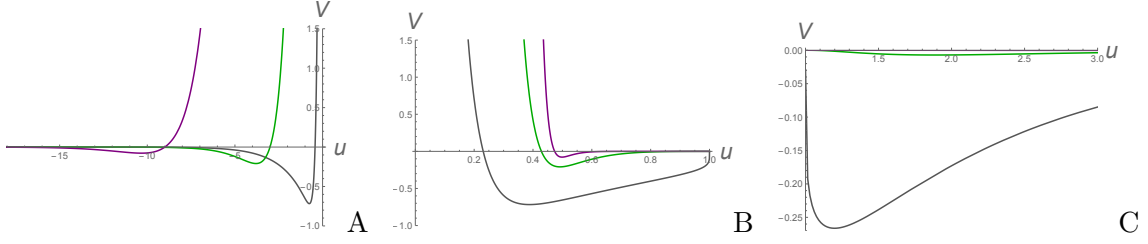


**Figure 4.** The potential as function of  $u$  at solutions presented in Fig. 3 for different  $k$  A)  $u < u_{02}$ ,  $u_{02} = 0$  B)  $u_{02} < u < u_{01}$ ,  $u_{01} = 1$ ,  $u_{02} = 0$  C)  $u > u_{01}$ ,  $u_{01} = 1$ . For all  $|E_1| = -|E_2| = -1$ ,  $C_1 = -C_2 = -1$ ,  $k = 0.4, 1, 1.2$ .

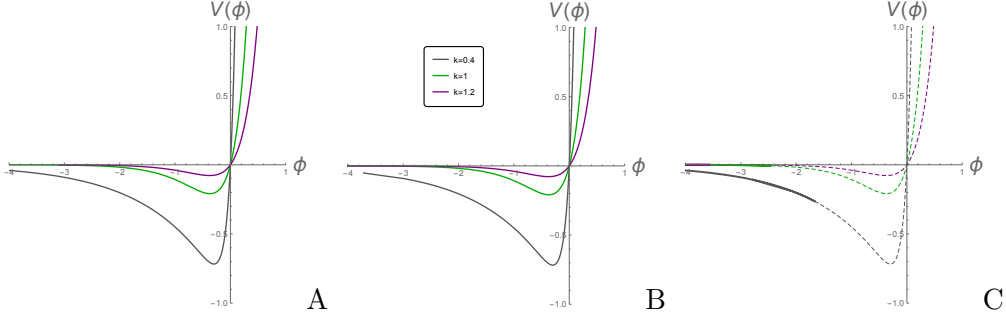


**Figure 5.** The dilaton potential plotted on solutions for  $\phi$ . A) The potential in the left-solution varies from  $V(\phi_1) = 0$  at  $\phi_1 = -\infty$ , reaches its minimum and then goes to  $V(\phi_2) = +\infty$  at  $\phi_2(u_{02} - \epsilon) = +\infty$  (thick lines). B) The potential on the middle solution varies from  $V(\phi_2) = +\infty$  at  $\phi_2 = \phi(u_{02} + \epsilon) = +\infty$  then reaches the minimal value  $V_{min} < 0$  and goes to  $V(\phi_1) = 0$  at  $\phi_1 = \phi(u_{01} - \epsilon) = -\infty$ . C) The potential of the right solution varies from  $V(\phi_1) = 0$  with  $\phi_1 = \phi(u_{01} + \epsilon) = -\infty$  to  $V_s < 0$ ,  $V_s = V(\phi)$  at the point  $\phi = \phi_s$ . When  $\phi_s$  goes back to  $-\infty$  the potential goes from  $V_s = V(\phi_s)$  back to zero.

and we get

$$\frac{\tanh |\mu_1(u_s - u_{01})|}{\tanh |\mu_2(u_s - u_{02})|} = \frac{\mu_1}{\mu_2}. \quad (3.23)$$

In Fig. 6 we observe that the extremal point of  $\phi(u)$  coincides with the extremal point of  $V(u)$ ,  $V'_u = V'_\phi \phi'_u$ . Note that the last does not coincide with an extremal point of  $V(\phi)$ .

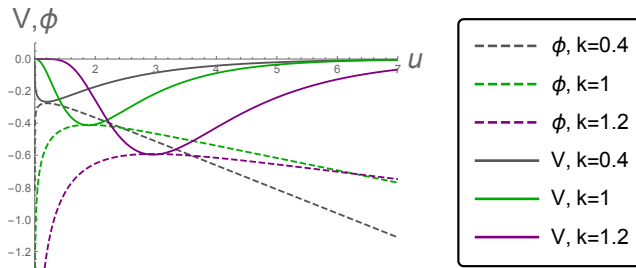


**Figure 6.** The rescaled potential and dilaton as functions of  $u$  in the right solution,  $u > u_{01}$ . We see that  $V'_u|_{u=u_s} = 0$  corresponds to  $\phi'_u|_{u=u_s} = 0$

The latter can also be computed analytically. Using

$$V'_\phi = 2k_1 C_1 e^{2k_1 \phi} + 2k_2 C_2 e^{2k_2 \phi}, \quad (3.24)$$

and taking into account that  $C_1 C_2 < 0$ , we can find

$$\phi_c = \frac{9k}{(16 - 9k^2)} \log \frac{3k}{4} + \frac{9k}{2(16 - 9k^2)} \log \left| \frac{C_1}{C_2} \right|. \quad (3.25)$$

We show the behaviour of the potential as a function of  $\phi$  and the dilaton as a function of  $u$  on the same plot in Fig. 7. In this picture we draw the dependences for all solutions.

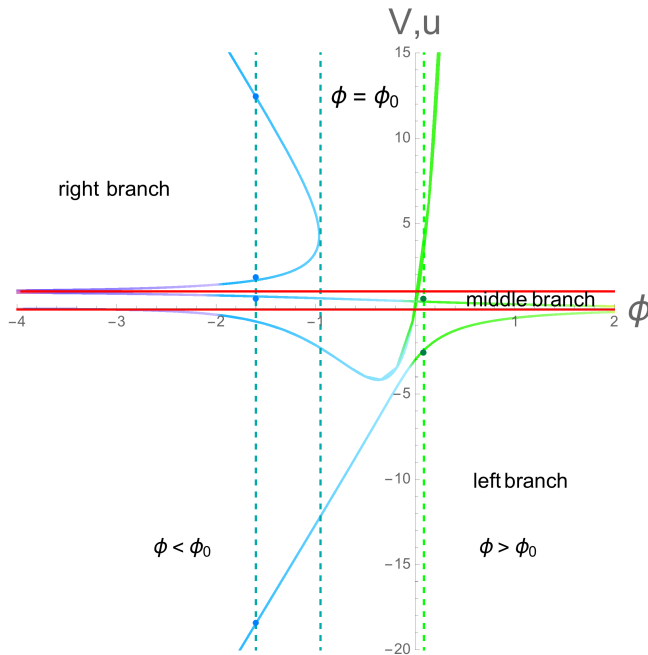


**Figure 7.** The dilaton potential  $V = V(\phi)$  on the vacuum solutions  $\phi = \phi(u)$  with (3.5)-(3.7) and plots that indicate which values of  $u$  correspond to given  $\phi$ , i.e.  $u = u(\phi)$ . The functions  $u(\phi)$  are different on the different branches, and moreover this functions is double-valued at the right branch. The different values of  $u$  corresponding to the same  $\phi$  are indicated by points at the vertical lines.

### 3.2.1 Special case, solutions with $u_{01} = u_{02}$

The 3-branch solutions for the metric (3.2) and the dilaton (3.3) can be reduced to the 2-branch solutions by putting  $u_{01} = u_{02} = u_0$ . In Fig. 8 the behavior of the dilaton (2.46) with  $u_{01} = u_{02} = u_0$  is shown. From this picture one can see that the dilaton tends to  $-\infty$  as  $u \rightarrow \pm\infty$ .

Let's find the asymptotics of the solution given by (3.2) and (3.3) with  $u_{01} = u_{02} = u_0$ . As for the previous metric solutions we perform these in the conformal coordinates.

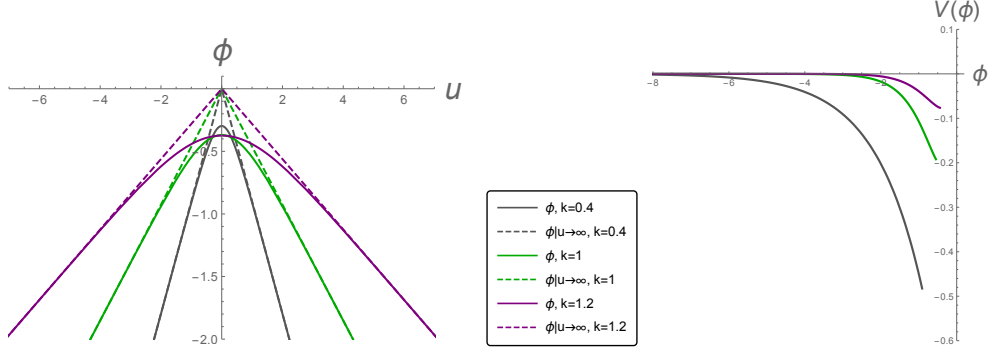


**Figure 8.** A) The behaviour of the dilaton (solid lines) and its asymptotics at infinity (dashed lines) for  $u_{01} = u_{02} = 0$ ,  $C_1 = -C_2 = -1$ ,  $|E_1| = -|E_2| = -1$  and different values of  $k$ . From bottom to top  $k = 0.4, 1, 1.2$ . B) The dilaton potential as a function of  $\phi$  for  $u > 0$ .

- In the limit with  $u \rightarrow \pm\infty$

$$ds^2 \sim z^{2/3}(-dt^2 + dy_1^2 + dy_2^2 + dy_3^2 + dz^2), \quad (3.26)$$

$$\phi|_{u \rightarrow \pm\infty} \sim \frac{9k}{9k^2 - 16}(\mu_2 - \mu_1)u \sim \log z \rightarrow -\infty, \quad (3.27)$$

where the conformal radial coordinate is given by  $z \sim \frac{4+3k}{3\mu_1} e^{\frac{3\mu_1 u}{4+3k}}$ . So we come to the same asymptotics as for the right (3.18) and left (3.10) solutions with  $u \rightarrow \pm\infty$  for the 3-branch case. The scalar curvature has also a common behaviour the right and left solutions and with  $u \rightarrow +\infty$  goes to infinity (A.27).

- For  $u \rightarrow u_0$  one gets has the following form of the metric (3.2)

$$ds^2 \sim \frac{1}{z^2}(-dt^2 + dy_1^2 + dy_2^2 + dy_3^2 + dz^2), \quad (3.28)$$

where the conformal "radial" coordinate is defined as  $z = 4(u - u_0)^{1/4}$  and  $z \rightarrow 0$  as  $u \rightarrow u_0$ . In (3.28) one can easily recognize the 5d AdS metric supported by the constant dilaton

$$\phi|_{u \rightarrow u_0} = \frac{9k}{(16 - 9k^2)} \log \frac{3k}{4} + \frac{9k}{2(16 - 9k^2)} \log \left| \frac{C_1}{C_2} \right| \quad (3.29)$$

which coincides with the minimum of the potential (3.25).

As expected the scalar curvature of this solution with  $u \rightarrow u_0$  has a constant value (A.26).

We note that the Fig. 8 is an agreement with calculations of the asymptotics for the dilaton.

The potential of the dilaton as function of  $\phi$  with  $u_{01} = u_{02} = u_0$  is presented in Fig. 8 B. From this plot we observe the existence of the turning point of the two-branch solution. The equation for the stop point (3.23) in this case becomes

$$\frac{\tanh(\mu_1(u_s - u_0))}{\tanh(\mu_2(u_s - u_0))} = \frac{\mu_1}{\mu_2}, \quad (3.30)$$

and has a solution

$$u_s = u_0. \quad (3.31)$$

As already observed, in this case we find that the stop point coincides with the critical point of the potential,  $\phi_s = \phi_c = \phi(u_0)$ .

#### 4 Non-vacuum solutions

In this section we examine non-vacuum case of the solution to the model (2.1). The metric and the dilaton are

$$ds^2 = F_1^{\frac{8}{9k^2-16}} F_2^{\frac{9k^2}{2(16-9k^2)}} \left( -e^{2\alpha^1 u} dt^2 + e^{-\frac{2\alpha^1}{3}u} d\vec{y}^2 \right) + F_1^{\frac{32}{9k^2-16}} F_2^{\frac{18k^2}{16-9k^2}} du^2, \quad (4.1)$$

$$\phi = -\frac{9k}{9k^2-16} \ln F_1 + \frac{9k}{9k^2-16} \ln F_2, \quad (4.2)$$

with

$$F_1 = \sqrt{\left| \frac{C_1}{2E_1} \right|} \sinh(\mu_1 |u - u_{01}|), \quad \mu_1 = \sqrt{\left| \frac{3E_1}{2} \left( k^2 - \frac{16}{9} \right) \right|}, \quad (4.3)$$

$$F_2 = \sqrt{\left| \frac{C_2}{2E_2} \right|} \sinh(\mu_2 |u - u_{02}|), \quad \mu_2 = \sqrt{\left| \frac{3E_2}{2} \left( \left( \frac{16}{9} \right)^2 \frac{1}{k^2} - \frac{16}{9} \right) \right|}. \quad (4.4)$$

Just as in the vacuum case, we need to separate the solutions in branches (3.5)-(3.9) with respect to values of  $u_{01}$  and  $u_{02}$ . We recall that  $E_1$  and  $E_2$  must obey the constraint

$$E_1 + E_2 + \frac{2}{3}(\alpha^1)^2 = 0. \quad (4.5)$$

The factors of  $\alpha^1$  in the metric (4.1) break the Poincaré symmetry. However, the presence of this parameter allows us to construct black branes.

##### 4.1 Black branes

Here we show that the metrics for the non-vacuum case (4.1)-(4.5) correspond to black branes. We present black-brane solutions in the IR and UV limits in conformal coordinates. One can present the metric (4.1) in the following form

$$ds^2 = e^{2A - \frac{2}{3}\alpha^1 u} \left( -e^{\frac{8}{3}\alpha^1 u} dt^2 + d\vec{y}^2 + e^{6A + \frac{2}{3}\alpha^1 u} \left( \frac{du}{dz} \right)^2 dz^2 \right) \quad (4.6)$$

where

$$e^{2A} = F_1^{\frac{8}{9k^2-16}} F_2^{\frac{9k^2}{2(16-9k^2)}}, \quad (4.7)$$

and  $F_1$  and  $F_2$  are given by (4.3)-(4.4). In (4.6) the  $z$ -variable is a new coordinate defined by

$$z - z_0 = \int_{u_0}^u e^{\frac{5}{3}\alpha^1 u} e^{3A} du, \quad (4.8)$$

or in the detailed form plugging  $A$  from (4.7) one gets

$$z - z_0 = \int_{u_0}^u e^{\frac{5}{3}\alpha^1 u} F_1^{\frac{12}{9k^2-16}} F_2^{\frac{27k^2}{4(16-9k^2)}}. \quad (4.9)$$

#### 4.1.1 Black brane in the IR-limit

The IR-limit corresponds to  $u \rightarrow +\infty$  ( $u \rightarrow -\infty$ ) for the right (left) solution of the chart (3.6) and the particular case (3.9) with  $u_{01} = u_{02}$ . Since  $u \rightarrow +\infty$  in  $F_1$  and  $F_2$  (4.3)-(4.4) only one exponential function survives and we have for (4.9)

$$z - z_0 = C \int_0^u e^{\frac{5}{3}\alpha^1 u} e^{\frac{3(9k^2\mu_2-16\mu_1)u}{4(16-9k^2)}} du, \quad (4.10)$$

where  $C$  is some constant. Integrating the  $r$ -coordinate takes the form

$$z = \frac{C}{\tilde{A}} e^{\tilde{A}u}, \quad (4.11)$$

with

$$\tilde{A} = \frac{5}{3}\alpha^1 + \frac{3(9k^2\mu_2-16\mu_1)}{4(16-9k^2)}, \quad (4.12)$$

and we also put  $z_0$  to be equal to an integration constant. So the  $z$ -coordinate (4.11) tends to  $\infty$  as  $u \rightarrow \infty$ .

The blackening function in (4.6) is

$$f = e^{\frac{8}{3}\alpha^1 u} = z^{\frac{8\alpha^1}{3\tilde{A}}} \quad (4.13)$$

with  $\alpha^1 < 0$  for  $u \rightarrow +\infty$  ( $\alpha^1 > 0 - u \rightarrow -\infty$ ).

The metric (4.6) comes to the form

$$ds^2 = \tilde{C} z^{\left(\frac{9k^2\mu_2-16\mu_1}{2(16-9k^2)} - \frac{2}{3}\alpha^1\right)\frac{1}{\tilde{A}}} \left( -z^{\frac{8\alpha^1}{3\tilde{A}}} dt^2 + dy_1^2 + dy_2^2 + dy_3^2 + \frac{dz^2}{z^{\frac{8\alpha^1}{3\tilde{A}}}} \right), \quad (4.14)$$

where we define

$$\tilde{C} = \left( \sqrt{\left| \frac{3C_1}{4} \left( k^2 - \frac{16}{9} \right) \right|} \right)^{\frac{8}{9k^2-16}} \left( \sqrt{\left| C_2 \left( \frac{64}{27k^2} - \frac{4}{3} \right) \right|} \right)^{\frac{9k^2}{2(16-9k^2)}}. \quad (4.15)$$

In the metric (4.14) one can recognize a black brane taken in the near-horizon limit.

The temperature of the black brane is

$$T = \frac{1}{4\pi} |f'|_{r=r_h} \sim \frac{2}{3\pi} \frac{\alpha^1}{\tilde{A}}. \quad (4.16)$$

For the particular case when the dilaton is constant at  $u \rightarrow \infty$  one needs to put  $\mu_1 = \mu_2$  and the metric (4.14) Taking into account the expression for  $\mu_2$  and for  $E_2$  (4.40) one can find out that  $\mu_1 = \frac{4}{3} |\alpha^1|$  and (4.1) comes to the form

$$ds^2 = -e^{\frac{8}{3}\alpha^1 u} dt^2 + d\vec{y}^2 + e^{-\frac{8}{3}\alpha^1 u} du^2. \quad (4.17)$$

or in the conformal coordinate (4.11)

$$ds^2 = \tilde{C} \left( -z dt^2 + dy_1^2 + dy_2^2 + dy_3^2 + \frac{dz^2}{z} \right). \quad (4.18)$$

#### 4.1.2 Black brane in the UV-limit

A black brane metric in the UV limit can be found in the case of the chart (3.9) with  $u_{01} = u_{02} = u_0$ . The UV limit corresponds to  $u \rightarrow u_0$ .

Expanding the integrand of (4.11) on  $u$ , the  $z$ -coordinate takes the following form

$$z - z_0 = \mathcal{C} \int_0^u du e^{\frac{5}{3}\alpha^1 u} (u - u_0)^{-\frac{3}{4}} \left( 1 + \frac{E_1 + E_2}{3} (u - u_0)^2 + \dots \right), \quad (4.19)$$

where

$$\mathcal{C} = 2^{\frac{3(27k^2+16)}{8(16-9k^2)}} 3^{\frac{3(9k^2+16)}{8(9k^2-16)}} |C_1|^{\frac{6}{9k^2-16}} |C_2|^{\frac{27k^2}{8(16-9k^2)}} k^{\frac{12}{9k^2-16}} \left( \frac{16-9k^2}{9k^2} \right)^{-\frac{3}{8}}. \quad (4.20)$$

Integrating (4.19) with  $u \rightarrow u_0$ , and with an appropriate choice of  $z_0$ , we find

$$z = 4\mathcal{C}(u - u_0)^{\frac{1}{4}}. \quad (4.21)$$

Now one can represent (4.6) in the following form

$$ds^2 = \Phi(z) \left( -f(z) dt^2 + dy_2^2 + dy_2^2 + dy_3^2 + \frac{dz^2}{f(z)} \right), \quad (4.22)$$

where the blackening function is

$$f = e^{-\frac{8|\alpha^1|}{3} \left( \frac{z}{4\mathcal{C}} \right)^4} \approx 1 - \frac{8|\alpha^1|}{3(4\mathcal{C})^4} z^4. \quad (4.23)$$

The conformal factor in (4.22) reads

$$\Phi(z) = e^{2A - \frac{2}{3}\alpha^1 u} \approx \tilde{C} \left[ \left( \frac{z}{4\mathcal{C}} \right)^{-2} + \frac{2|\alpha^1|}{3} \left( \frac{z}{4\mathcal{C}} \right)^2 \right], \quad (4.24)$$

with  $\tilde{C}$  given by (4.15).

The dilaton field which supports the black brane in the UV is

$$\phi = \frac{9}{16-9k^2} \ln \left( \frac{\mu_2}{\mu_1} \right) + \frac{9}{2(16-9k^2)} \log \left( \frac{C_1 E_2}{C_2 E_1} \right). \quad (4.25)$$

It worth to be noted that since  $z$  is also small, one can neglect the second term into the brackets in (4.24). So the black brane metric (4.22) can rewritten as

$$ds^2 = C \left( \frac{4\mathcal{C}}{z} \right)^2 \left[ - \left( 1 - \frac{8|\alpha^1|}{3(4\mathcal{C})^4} z^4 \right) dt^2 + dy_2^2 + dy_2^2 + dy_3^2 + \frac{dz^2}{1 - \frac{8|\alpha^1|}{3(4\mathcal{C})^4} z^4} \right], \quad (4.26)$$

that is the well-known form of the 5d black brane in the AdS spacetime.

The horizon of the black brane is at

$$z_h = \left( \frac{3}{8|\alpha^1|} \right)^{1/4} 4\mathcal{C}, \quad (4.27)$$

and the temperature in this case is

$$T = \frac{1}{4\pi C} \left( \frac{8|\alpha^1|}{3} \right)^{1/4}. \quad (4.28)$$

## 4.2 The asymptotics of the metric and the dilaton

We consider here the asymptotics of the dilaton (4.2) and metric near the boundaries of 3 branches solutions with (3.5)-(3.7).

### The left solution

- at  $u \rightarrow -\infty$  the asymptotics of the metric (4.1) is given by (4.14). The parameter  $\alpha^1$  can be as positive as negative, in the case of positive values the background describe a black brane. The dilaton that supports this geometry is

$$\phi_{u \rightarrow -\infty} = \frac{9k}{16 - 9k^2} \left[ (\mu_2 - \mu_1) u + \frac{1}{2} \log \left| \frac{C_2 E_1}{C_1 E_2} \right| \right] \rightarrow -\infty, \quad (4.29)$$

$$\sim \frac{9k}{16 - 9k^2} \left[ \frac{(\mu_2 - \mu_1)}{\tilde{A}} \log(\tilde{A}z) + \frac{1}{2} \log \left| \frac{C_2 E_1}{C_1 E_2} \right| \right] \rightarrow -\infty, \quad (4.30)$$

where the conformal coordinate  $z$  is given by (4.11) and the parameter  $\tilde{A}$  by (4.12).

- at  $u \rightarrow u_{02} - \epsilon$  the metric (4.1) takes the form

$$ds^2 \sim z^{\frac{18k^2}{64-9k^2}} \left( e^{2\alpha^1 u_{02}} (-dt^2 + dy_1^2) + e^{-\frac{2\alpha^1}{3} u_{02}} (dy_2^2 + dy_3^2) + dz^2 \right), \quad (4.31)$$

since  $u_{02}$  is some constant this asymptotics matches with the vacuum one (3.12) and the dilaton

$$\phi_{u \rightarrow u_{02} - \epsilon} = -\frac{9k}{16 - 9k^2} \log \left[ \sqrt{\frac{C_2 E_1}{C_1 E_2}} \frac{\mu_2 \epsilon}{\sinh(|\mu_1 (u_{01} - u_{02})|)} \right] \rightarrow +\infty. \quad (4.32)$$

### The middle solution

- at  $u \rightarrow u_{02} + \epsilon$  the asymptotics of the metric and the dilaton matches with those (4.31)-(4.32) for the left solutions

$$ds^2 \sim z^{\frac{18k^2}{64-9k^2}} \left( e^{2\alpha^1 u_{02}} (-dt^2 + dy_1^2) + e^{-\frac{2\alpha^1}{3} u_{02}} (dy_2^2 + dy_3^2) + dz^2 \right), \quad (4.33)$$

$$\phi_{u \rightarrow u_{02} + \epsilon} = -\frac{9k}{16-9k^2} \log \left[ \sqrt{\frac{C_2 E_1}{C_1 E_2}} \frac{\mu_2 \epsilon}{\sinh(\mu_1 (u_{01} - u_{02}))} \right] \rightarrow +\infty, \quad (4.34)$$

- at  $u \rightarrow u_{01} - \epsilon$  it is

$$ds^2 \sim z^{\frac{8}{9k^2-4}} (e^{2\alpha^1 u_{01}} (-dt^2 + dy_1^2) + e^{-\frac{2}{3}\alpha^1 u_{01}} (dy_2^2 + dy_3^2) + dz^2), \quad (4.35)$$

$$\phi_{u \rightarrow u_{01} - \epsilon} = -\frac{9k}{16-9k^2} \log \left[ \sqrt{\frac{C_2 E_1}{C_1 E_2}} \frac{\sinh(|\mu_2 u_{01} - u_{02}|)}{\mu_1 \epsilon} \right] \rightarrow -\infty. \quad (4.36)$$

Here we again can see that the asymptotics of the metrics match with the vacuum ones (3.12)-(3.15) for the middle branch.

### The right solution

- at  $u \rightarrow u_{01} + \epsilon$  the asymptotics of the geometry of the dilaton are those for the middle solution at  $u \rightarrow u_{01} - \epsilon$  (4.35)-(4.36). This limit coincides with the corresponding vacuum asymptotics.
- at  $u \rightarrow +\infty$  the asymptotics
- for the limit  $u \rightarrow \infty$  the asymptotic metric has the same form as (4.14), and one can determine a black brane if  $\alpha^1$  is negative. It is supported by the dilaton

$$\phi_{u \rightarrow \infty} = -\frac{9k}{16-9k^2} \left[ (\mu_2 - \mu_1) u + \frac{1}{2} \log \left| \frac{C_2 E_1}{C_1 E_2} \right| \right] \rightarrow -\infty, \quad (4.37)$$

$$\sim -\frac{9k}{16-9k^2} \left[ \frac{(\mu_2 - \mu_1)}{\tilde{A}} \log(\tilde{A}z) + \frac{1}{2} \log \left| \frac{C_2 E_1}{C_1 E_2} \right| \right]. \quad (4.38)$$

In (4.38) we used  $z$  given by (4.11) and the parameter  $\tilde{A}$  by (4.12).

At first sight, the asymptotics of the dilaton (4.29) and (4.37) are the same as for the vacuum case (3.11) and (3.19). However, since the parameter  $\alpha^1$  enters the game and we have the constraint (4.5),  $\mu_1$  can be greater than  $\mu_2$ . This will change the asymptotics of the dilaton for (4.29) and (4.37) at  $u \rightarrow \pm\infty$  from  $-\infty$  to  $+\infty$ .

Moreover the equality

$$\mu_1 = \mu_2, \quad (4.39)$$

can be obtained with

$$E_2 = \frac{6k^2(\alpha^1)^2}{16-9k^2}. \quad (4.40)$$

This (4.39) allows us to reach a constant value for the dilaton at  $u \rightarrow \pm\infty$  (4.29) and (4.37). In particular, in the case of black branes, we can assure that the dilaton remains finite at the horizon for any temperature.

We illustrate the behaviour of the dilaton solution for the non-vacuum case in Fig. 9. As it was expected the condition (4.5) changes the behaviour of the dilaton. In Fig. 9 B) we plot the dilaton keeping the same shape of the potential and the value of  $\alpha^1$  as for Fig. 9 A), but the values of the parameter  $E_2$  are changed with respect to (4.40). In Fig. 9 C) we again save the form of the potential, use the same value of  $E_2$  as in A), take bigger  $\alpha^1$  and show that the opposite sign of this parameter doesn't change the asymptotics of the dilaton. From Fig. 9 C) one observes that for  $u \rightarrow \pm\infty$   $\phi$  can tend to  $+\infty$ , while for the vacuum case  $\phi \rightarrow -\infty$  as  $u \rightarrow \pm\infty$ , that confirms our discussion of the analytical results for the dilaton asymptotics.

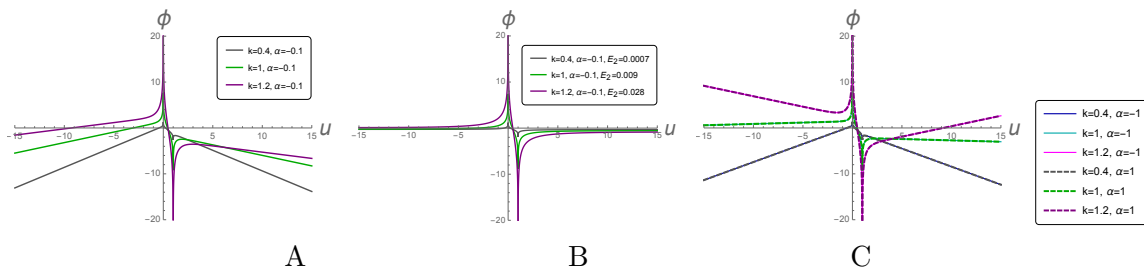


**Figure 9.** The behaviour of the dilaton solution for the 3-branch solutions with  $u_{01} = 1, u_{02} = 0$ , the non-vacuum case: A)  $\alpha^1 = -0.1, E_2 = 1, k = 0.4, 1, 1.2$ ; B)  $E_2 = 0.0007$  for  $k = 0.4, E_2 = 0.009$  for  $k = 1, E_2 = 0.028$  for  $k = 1.2; C_1 = -1, C_2 = 1, \alpha^1 = -0.1$ , for all; C) solid lines -  $\alpha^1 = -1$ , dashed lines -  $\alpha^1 = 1, k = 0.4, 1, 1.2, C_1 = -1, C_2 = 1, E_2 = 1$  for all.

In Fig. 10 we draw the potential  $V$  as a function of  $\phi$  and the dependence  $u$  on  $\phi$ . The functions  $u(\phi)$  are different on the different branches. The different values of  $u$  corresponding to the same  $\phi$  are indicated by points at the vertical lines. We see that the function  $u(\phi)$  for  $|\alpha^1| < \alpha_{cr}^1$  is double-valued on the right branch, and for  $|\alpha^1| > \alpha_{cr}^1$  it is double-valued on the left branch, and for  $|\alpha^1| = \alpha_{cr}^1$  the both functions one-to-one functions for all branches, and  $\phi < \phi'_0$  for the right branch and  $\phi > \phi''_0$  at the left branch.

### 4.3 The special case $u_{01} = u_{02}$

Let's turn to the special case of the non-vacuum solution with  $u_{01} = u_{02} = u_0$ . The metric and the dilaton have the following limits:

- for  $u \rightarrow \infty$  the metric is described by that one obtained for the 3-branch solutions (4.14) by putting  $u_{01} = u_{02} = u_0$ , with the appropriate choice of the parameter  $\alpha^1$  it can describe a black brane in the IR-limit. This geometry is supported by the dilaton

$$\phi|_{u \rightarrow \pm\infty} \sim \frac{9k}{9k^2 - 16} \left[ \pm (\mu_2 - \mu_1) u + \frac{1}{2} \log \left| \frac{C_2 E_1}{C_1 E_2} \right| \right], \quad (4.41)$$

$$\sim \frac{9k}{9k^2 - 16} \left[ \pm \frac{(\mu_2 - \mu_1)}{\tilde{A}} \log \tilde{A} z + \frac{1}{2} \log \left| \frac{C_2 E_1}{C_1 E_2} \right| \right], \quad (4.42)$$

where in (4.42) we used (4.11) and (4.12).

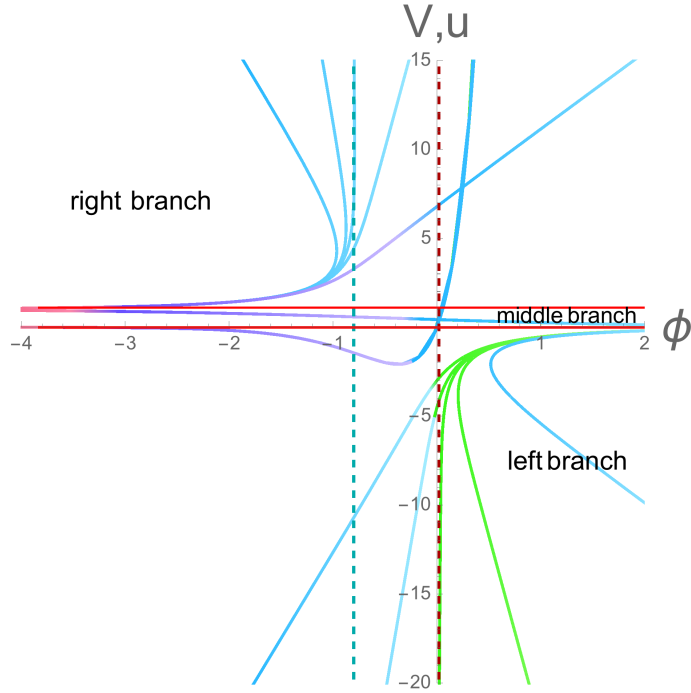


**Figure 10.** The dilaton potential  $V = V(\phi)$  on non-vacuum solutions  $\phi = \phi(u)$  with (3.5)-(3.7) and plots that indicate which values of  $u$  correspond to given  $\phi$ , i.e.  $u = u(\phi)$ .

- as for  $u \rightarrow +0$  we have a black brane (4.22)-(4.24) in the UV-limit with the constant dilaton

$$\phi|_{u \rightarrow u_0} = \frac{9}{16 - 9k^2} \log\left(\frac{\mu_2}{\mu_1}\right) + \frac{9}{2(16 - 9k^2)} \log\left(\frac{C_1 E_2}{C_2 E_1}\right). \quad (4.43)$$

The calculations of the asymptotics for the dilaton are confirmed by the behaviour of the dilaton in Fig. 11. It should be noted that near  $u = u_0$  the dilaton is also constant, that can be seen, for example from Fig. 11A).

In Fig. 11 we plot the dependences of the dilaton solution with  $u_{01} = u_{02} = u_0$  on  $u$  (3.9). As for the 3-branch solutions from Fig. 11 B) we see that the dilaton can be constant with the appropriate choice of parameters agreed with (4.5) and can change its asymptotics from  $-\infty$  to  $+\infty$  at  $u \rightarrow \pm\infty$ , see Fig. 11 C).

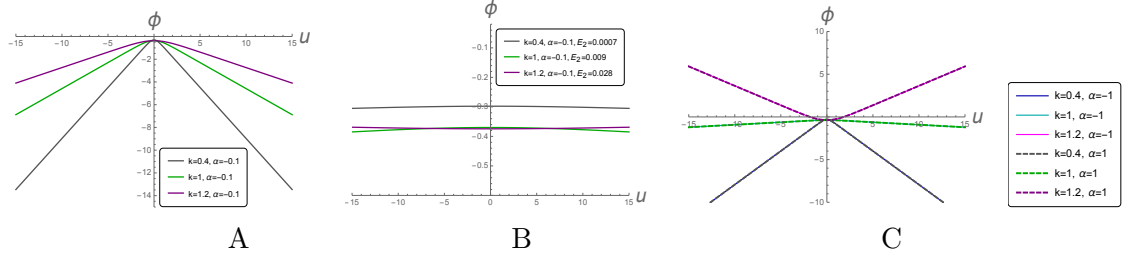


**Figure 11.** The behaviour of the dilaton solution for the 2-branch solutions, the non-vacuum case: A)  $\alpha^1 = -0.1$ ,  $E_2 = 1$ ,  $k = 0.4, 1, 1.2$ , B)  $E_2 = 0.0007$  for  $k = 0.4$ ,  $E_2 = 0.009$  for  $k = 1$ ,  $E_2 = 0.028$  for  $k = 1.2$ ;  $C_1 = -1$ ,  $C_2 = 1$ ,  $\alpha^1 = -0.1$  for all; C) solid lines –  $\alpha^1 = -1$ , dashed lines –  $\alpha^1 = 1$ ,  $k = 0.4, 1, 1.2$ ,  $C_1 = -1$ ,  $C_2 = 1$ ,  $E_2 = 1$  for all.

## 5 Holographic RG flows

In this section we study our solutions as holographic RG flows. It is useful to come to so-called domain wall coordinates. In this coordinates a general form of the non-vacuum solutions is

$$ds^2 = \frac{dw^2}{f(w)} + e^{2\mathcal{A}(w)} (-f(w)dt^2 + \eta_{ij}dx^i dx^j), \quad (5.1)$$

which covers the vacuum case with  $f(w) = 1$ . Both temperature and vacuum solutions are characterized by the metric scale factor  $e^{\mathcal{A}(w)}$ , that measures the field theory energy scale, the blackening function  $f(w)$  and by a scalar field profile  $\phi(w)$

$$\lambda = e^\phi, \quad (5.2)$$

which is interpreted as the running coupling.

One can define the  $\beta$ -function holographically as

$$\beta(\lambda) = \frac{d\lambda}{d \log E} = \frac{d\lambda}{d\mathcal{A}}. \quad (5.3)$$

In general case the  $\beta$ -function satisfies the following RG equations

$$\frac{dX}{d\phi} = -\frac{4}{3} (1 - X^2 + Y) \left( 1 + \frac{3}{8X} \frac{d \log V}{d\phi} \right), \quad (5.4)$$

$$\frac{dY}{d\phi} = -\frac{4}{3} (1 - X^2 + Y) \frac{Y}{X}, \quad (5.5)$$

where  $X(\phi)$  is related with the  $\beta$ -function

$$X(\phi) = \frac{\beta(\lambda)}{3\lambda}, \quad (5.6)$$

or plugging the RHS of (5.3) into (5.6)

$$X = \frac{1}{3\lambda} \frac{d\lambda}{d\mathcal{A}}. \quad (5.7)$$

In eqs. (5.4)-(5.5) the  $Y$ -variable is defined through the function  $f$

$$Y(\phi) = \frac{1}{4} \frac{g'}{\mathcal{A}'}, \quad g = \log f, \quad (5.8)$$

representing the relation with the finite temperature. If the vacuum case is considered the function  $Y$  vanishes and the system (5.4)-(5.5) reduces to one equation

$$\frac{dX}{d\phi} = -\frac{4}{3} (1 - X^2) \left( 1 + \frac{3}{8X} \frac{d \log V}{d\phi} \right). \quad (5.9)$$

One can study eqs.(5.4)-(5.5) as a nonautonomous dynamical system using just a relation for the dilaton potential. In particular, it is possible to use the notion of the superpotential and its appropriate behaviour. This approach was elaborated in details in works [5, 11, 14]. At the same, knowing exact solutions for the dilaton and the scale factor, we can directly explore the behaviour of the functions (5.6)-(5.8).

### 5.1 The domain-wall coordinates

For convenience we write down the metric of the solutions. For the vacuum case it reads

$$ds^2 = F_1^{\frac{8}{9k^2-16}} F_2^{\frac{9k^2}{2(16-9k^2)}} \left[ -dt^2 + dy_1^2 + dy_2^2 + dy_3^2 \right] + F_1^{\frac{32}{9k^2-16}} F_2^{\frac{18k^2}{16-9k^2}} du^2, \quad (5.10)$$

while for the non-vacuum one

$$ds^2 = F_1^{\frac{8}{9k^2-16}} F_2^{\frac{9k^2}{2(16-9k^2)}} e^{-\frac{2}{3}\alpha^1 u} \left[ -e^{\frac{8}{3}\alpha^1 u} dt^2 + dy_1^2 + dy_2^2 + dy_3^2 \right] + F_1^{\frac{32}{9k^2-16}} F_2^{\frac{18k^2}{16-9k^2}} du^2, \quad (5.11)$$

where the functions  $F_1$  and  $F_2$  given by (2.48)-(2.49). For both cases the dilaton reads (2.46)

$$\phi = \frac{9k}{9k^2 - 16} \log \left( \frac{F_2}{F_1} \right) \quad (5.12)$$

and then we have

$$\lambda = \left( \frac{F_2}{F_1} \right)^{\frac{9k}{9k^2-16}}. \quad (5.13)$$

It worth to be noted that we should take into account our different coordinates for the solutions (3.5)-(3.9). The domain wall forms of the solutions (5.10)-(5.11) look correspondingly

$$ds^2 = e^{2\mathcal{A}} \left[ -dt^2 + dy_1^2 + dy_2^2 + dy_3^2 \right] + dw^2, \quad (5.14)$$

$$ds^2 = e^{2\mathcal{A}} \left[ -f dt^2 + dy_1^2 + dy_2^2 + dy_3^2 \right] + \frac{dw^2}{f}, \quad (5.15)$$

where the function  $f$  defined by

$$f = e^{\frac{8}{3}\alpha^1 u}. \quad (5.16)$$

To come to (5.14)-(5.15) we use the change of variables for (5.10)-(5.11)

$$vac : \quad dw = F_1^{\frac{16}{9k^2-16}} F_2^{\frac{9k^2}{16-9k^2}} du, \quad (5.17)$$

$$non - vac : \quad dw = F_1^{\frac{16}{9k^2-16}} F_2^{\frac{9k^2}{16-9k^2}} e^{\frac{4}{3}\alpha^1 u} du. \quad (5.18)$$

Generally we can represent the scale factor of the domain wall (5.14)-(5.15) as follows

$$\mathcal{A} = \frac{4}{9k^2-16} \log F_1 + \frac{9k^2}{4(16-9k^2)} \log F_2 - \frac{1}{3}\alpha^1 u, \quad (5.19)$$

so the energy scale  $A$  is

$$A \equiv e^{\mathcal{A}} = F_1^{\frac{4}{9k^2-16}} F_2^{\frac{9k^2}{4(16-9k^2)}} e^{-\frac{1}{3}\alpha^1 u}. \quad (5.20)$$

Putting  $\alpha^1 = 0$  in (5.19)-(5.20) one comes to the domain wall solution in the vacuum case (5.14). The function  $X$  (5.7) is represented as follows

$$X = \frac{1}{3} \left( \frac{F_2}{F_1} \right)^{\frac{9k}{16-9k^2}} \frac{\lambda'}{\mathcal{A}'}. \quad (5.21)$$

with  $\lambda$  given by (5.13),  $\mathcal{A}$  - by (5.19) and prime means the derivative with respect to  $u$

## 5.2 RG flow at zero-temperature

It is useful to explore the evolution of the rescaled  $\beta$ -function  $X$  (5.6) as a function of  $\log$  of the running coupling (5.2), which is the dilaton  $\phi$ . In Pic. 12 we present the behaviour of  $X$  (5.21) using solutions for  $\phi$  (5.12) and  $\mathcal{A}$  (5.19) with  $\alpha^1 = 0$  and (3.5)-(3.7). In these plots we fix the form of the potential putting  $C_1 = -C_2 = -2$  and  $k = 0.4$  while we vary the constants  $|E_1| = |E_2|$ . From Pic. 12 **A**) and **C**) we see that the holographic  $\beta$ -functions at zero temperature constructed on the left  $u < u_{02}$  and right solutions  $u > u_{01}$  can take both negative and positive values. As for the case **B**), which corresponds to the middle solution,  $X$  is always negative.

It is also of our interest to see the function  $X(\phi)$  plotted on the 2 branch solutions with  $u_{01} = u_{02} = u_0$ , particularly for  $u_0 = 0$ . In Fig. 13 we show the function  $X(\phi)$  on the dilation solution (5.12) with  $u_{01} = u_{02}$ . We see that the behaviour of the function  $X(\phi)$  is the same for all values of  $E_2$ . From Figs. 12-13 we see that  $X$  are regular except those plotted on the left solutions on Fig. 12 **A**) at some points  $\phi_s$  where  $X(\phi_s)$  takes an infinite value. From eq. (5.21) with  $\alpha^1 = 0$  one can understand that  $X$  is infinite with  $\mathcal{A}' = 0$ , i.e.

$$9k^2 \frac{F_2'}{F_2} - 16 \frac{F_1'}{F_1} = 0. \quad (5.22)$$

Eq. (5.22) defines the singular point  $u_s$ , which is related to  $\phi_s$ . The singular point  $\phi_s$  coincides with the point where  $\mathcal{A}' = 0$ , and its position depends on  $E, k, u_{01}$  and  $u_{02}$ , see Fig.14.

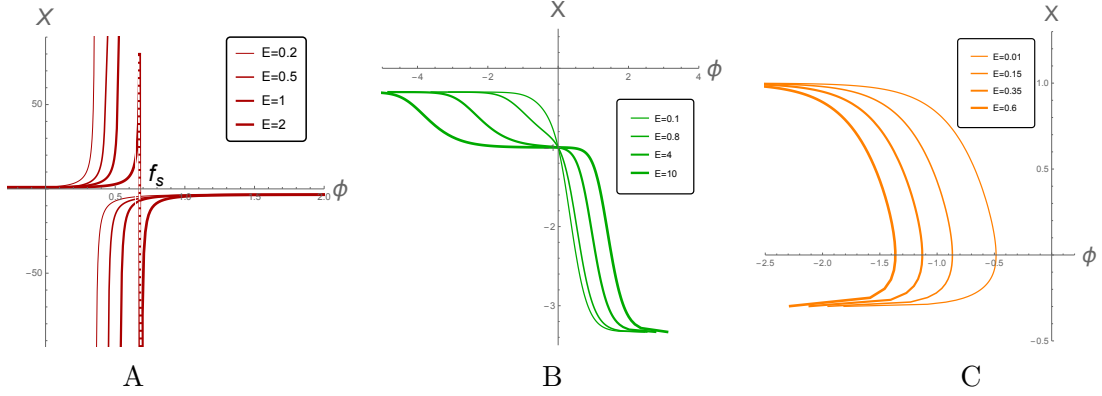


**Figure 12.** The behaviour of the  $X$ -function with the dependence on the dilaton plotted using the solutions for  $\mathcal{A}$  and  $\phi$ : A) the left branch with  $u_{02} > u$ , B) the middle branch  $u_{02} < u < u_{01}$ ; C) the right branch  $u > u_{01}$ . For all plots  $u_{01} = 1$ ,  $u_{02} = 0$ ,  $k = 0.4$ ,  $C_1 = -2$ ,  $C_2 = 2$ , different curves on the same plot correspond to the different values of  $|E_1| = |E_2|$ , labeled as  $E$  on the legends.

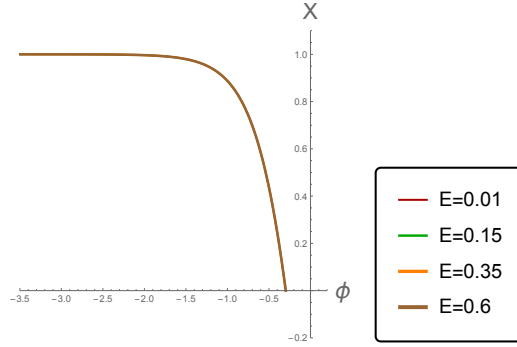


**Figure 13.** The  $X(\phi)$  function for the dilaton solution with  $u_{01} = u_{02} = 0$ , the potential fixed as  $C_1 = -2$ ,  $C_2 = 2$ ,  $k = 0.4$ . For all range of values of  $|E_1| = |E_2|$ , labeled as  $E$  on the legend, the curves of  $X$  coincide.

In the beginning of the section it was already said the system (5.4)-(5.5) the vacuum solutions comes to eq. (5.9), which is quite simple and one can treat it in the general form. We remind that the dilaton potential is given by

$$V = C_1 e^{2k_1 \phi} + C_2 e^{2k_2 \phi}, \quad (5.23)$$

or in the cases presented at the plots below

$$V = -2e^{2k\phi} + 2e^{\frac{32}{9k}\phi}, \quad (5.24)$$

with  $k = k_1$  and  $k_2 = \frac{16}{9k_1}$  (a constraint from the solution) and  $C_1 = -2$ ,  $C_2 = 2$ . The values of the dilaton coupling constant have the following restriction  $0 < k < 4/3$ .

Taking into account (5.24) we have

$$\frac{d \log V}{d\phi} = \frac{-2ke^{2k\phi} + \frac{32}{9k}e^{\frac{32}{9k}\phi}}{-e^{2k\phi} + e^{\frac{32}{9k}\phi}}. \quad (5.25)$$

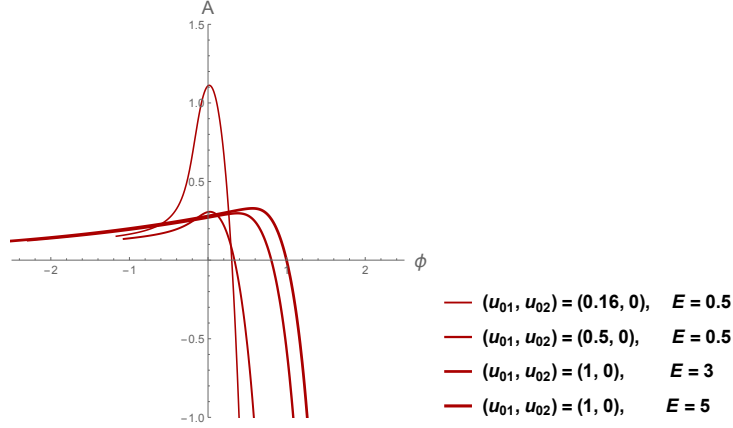


**Figure 14.** The behaviour of  $\mathcal{A} = \mathcal{A}(\phi)$  as a function of  $\phi$  for the vacuum solutions on (3.5)-(3.7). On the legends we present the values of chose  $u_{01}$ (the greater) and  $u_{02}$ (the smaller) and  $|E_1| = |E_2|$ , denoted as  $E$ .

The solution to (5.9) with (5.24)-(5.25) is represented in Fig. 15 using StreamPlot. On this figure we observe all possible solutions for  $X$  (blue curves) to our model with the potential (5.24). We also impose Figs. 12 and 13 on Fig. 15A) and see that they can partially cover the plot. In Fig. 15A) the red lines correspond to the left solution, see Fig. 12 A), the green lines are those from the middle solution, see Fig. 12 B), the orange ones correspond to the right solution, see Fig. 12 C). In Fig. 15 A) we observe that the function  $X$  corresponding to the right solution (the orange curves) interpolates between  $X_{c2}$  and 1. The  $X$  for the middle solution (the green curves) interpolates between  $X_{c1}$  and  $X_{c2}$  in Fig. 15. The dark red curves start at 1 and go to  $+\infty$  as  $\phi \rightarrow \phi_s - 0$ , some of these lines have local minimum and are located very closed to the brown curve corresponding to the vacuum flow for the two branch solution  $u_{01} = u_{02}t$ . The flow with local maximum in Fig. 15 A) corresponds to our solutions with small difference between  $u_{01}$  and  $u_{02}$ . The magenta lines start at  $X_{c1}$  and go to  $-\infty$  when  $\phi \rightarrow \phi_s + 0$ . For the fixed form of the potential the point  $\phi_s$  is defined by values of  $|E_1| = |E_2|$  (labeled by  $E$  on legend),  $u_{01}, u_{02}$ , i.e.  $\phi_s = \phi_s(E, u_{01}, u_{02})$ .

We see that in Fig. 15 A) some parts of the RG flow (the stream at the left bottom part as well as the stream at the right upper part that interpolates between  $-1$  and  $1$ ) are not covered by our vacuum solutions. However, it was already pointed in Sec. 2.2 that analytic solutions for  $\mathcal{A}$  and  $\phi$  can be governed by  $F_1$  and  $F_2$  that are *sin*- or linear functions, namely

$$F_1 = \sqrt{\left| \frac{C_1}{2E_1} \right|} \sin(\mu_1 |u - u_{01}|), \quad \mu_1 = \sqrt{\left| \frac{3E_1}{2} \left( k^2 - \frac{16}{9} \right) \right|}, \quad (5.26)$$

$$F_2 = \sqrt{\left| \frac{C_2}{2E_2} \right|} \sin(\mu_2 |u - u_{02}|), \quad \mu_2 = \sqrt{\left| \frac{3E_2}{2} \left( \left( \frac{16}{9} \right)^2 \frac{1}{k^2} - \frac{16}{9} \right) \right|}, \quad (5.27)$$

$$F_1 = \sqrt{\frac{3}{4} \left( k^2 - \frac{16}{9} \right)} C_1 (u - u_{01}), \quad F_2 = \sqrt{\frac{3}{4} \left( \left( \frac{16}{9k} \right)^2 - \frac{16}{9} \right)} C_2 (u - u_{02}), \quad (5.28)$$

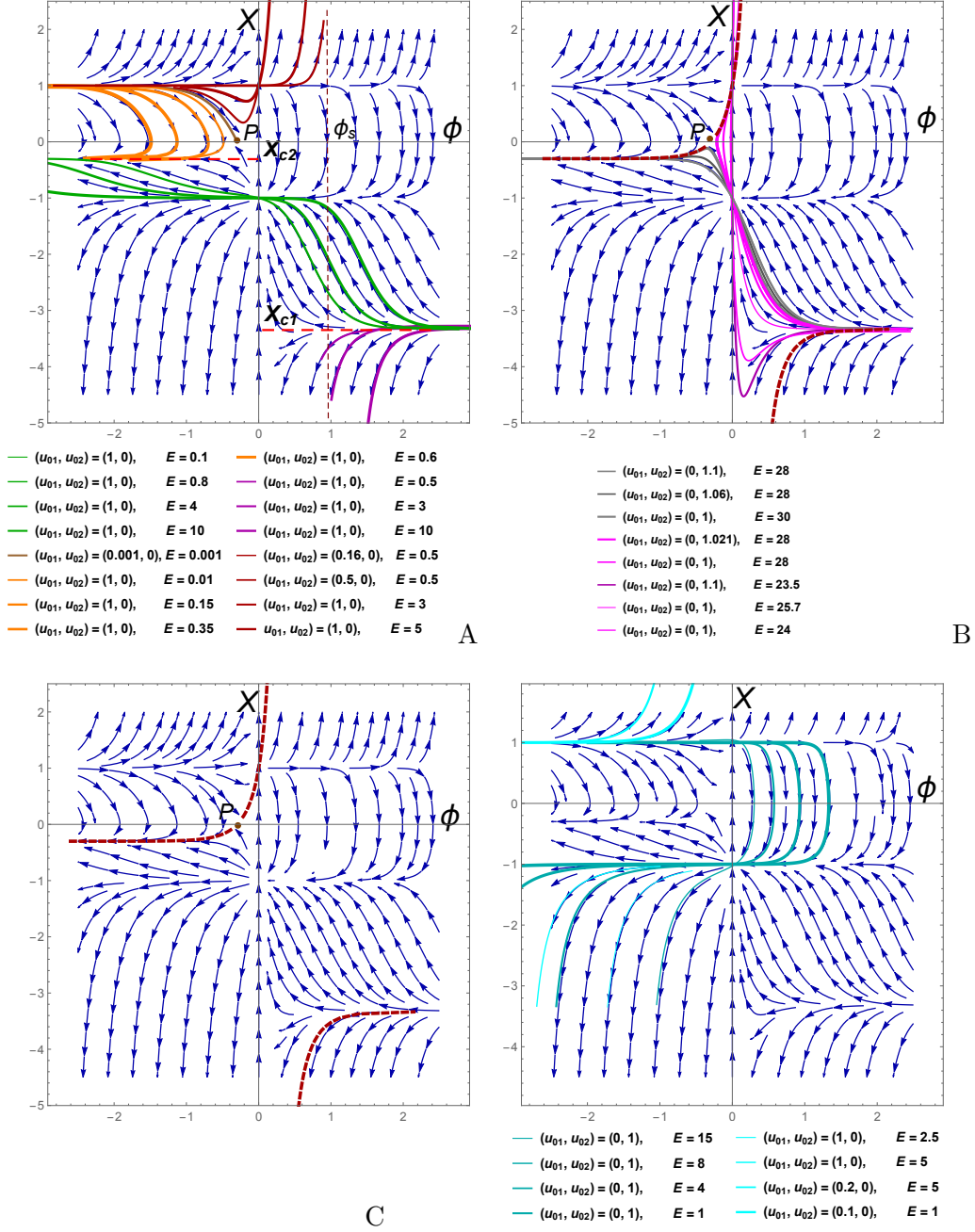


**Figure 15.** All solutions  $X$  to (5.9) (blue curves) with potential fixed as  $C_1 = -C_2 = -2$  and  $k = 0.4$ . **A)** The orange curves show  $X = X(\phi)$  plotted on the right solution, the green curves show  $X = X(\phi)$  on the middle one, the dark magenta and red lines show  $X = X(\phi)$  on the left solution. **B)** The magenta and grey curves show  $X = X(\phi)$  built on analytic solutions with sin-formula (5.26)-(5.27), the red dashed lines show  $X = X(\phi)$ , given by the "linear"-formula (5.28). **C)** Separately, the red lines show  $X = X(\phi)$  governed by "linear"-functions (5.28). **D)** As for the pictures A,B,C blue lines show the stream, that solves equation (5.9), while the lines of cyan and darker cyan lines present the behaviour of  $X(\phi)$  governed by *cosh* functions.

where in (5.26)-(5.27)  $E_1 > 0$ ,  $E_2 < 0$  with  $|E_1| = |E_2|$  and  $E_1 = E_2 = 0$  for (5.28). Since the equation (5.9) doesn't know about our choice of the solutions and we see on the plot all possible solutions, and the curves of the dependence  $X(\phi)$  on  $\phi$  built on (5.26)-(5.28) should appear on the plot. In Fig. 15 B) we present the stream of (5.9) by blue lines,  $X(\phi)$  on  $\phi$  plotted using (5.26)-(5.27) by magenta and grey lines and  $X(\phi)$  related to (5.28) by the dark red lines, correspondingly. We see that these lines partially fit the solutions to equation (5.9). We show separately the behaviour of  $X(\phi)$  with (5.28) in Fig. 15 C). From Fig. 15 A) and B) we see that  $X(\phi)$  corresponding to the linear solutions can be considered as a boundary between  $X(\phi)$  corresponding to "sin"-solutions and  $X(\phi)$  governed by the left *sinh*-solutions (i.e. *sinh*-solutions with  $u < u_{02}$ ).

However, we still observe in Fig. 15 B) and C) that some regions of the figure are not covered. If we look at the equation (5.9) it is evidently that it is invariant under the change of the sign of the potential (5.24), i.e.  $V \rightarrow -V$ . So the stream of eq.(5.9) should include also solutions to equations of motions with  $-V$ . In Sec. 2.2 we see that these are solutions with  $F_1$  and  $F_2$  governed by *cosh*-functions:

$$F_1 = \sqrt{\left| \frac{C_1}{2E_1} \right|} \cosh(\mu_1 |u - u_{01}|), \quad \mu_1 = \sqrt{\left| \frac{3E_1}{2} \left( k^2 - \frac{16}{9} \right) \right|}, \quad (5.29)$$

$$F_2 = \sqrt{\left| \frac{C_2}{2E_2} \right|} \cosh(\mu_2 |u - u_{02}|), \quad \mu_2 = \sqrt{\left| \frac{3E_2}{2} \left( \left( \frac{16}{9} \right)^2 \frac{1}{k^2} - \frac{16}{9} \right) \right|}, \quad (5.30)$$

with  $C_1 > 0$ ,  $C_2 < 0$ ,  $E_1 < 0$ ,  $E_2 > 0$ . In Fig. 15 D) we draw  $X(\phi)$  as a solution to (5.9) (blue lines) and with the help of the analytical solution related to (5.29)-(5.30) (the curves of other colors), that perfectly complete the necessary part of the stream.

Let's look at Figs. 15 A) and B) more closely. On these pictures we see a special point  $P$ , which is a stationary point of our potential  $V'(\phi) = 0$ . We zoom the scale near the point  $P$  in Fig. 16 to see the behaviour of the vacuum  $X(\phi)$  functions near  $P$  in details. As in the previous figures we show the stream of eq.(5.9) by blue curves and by the other color curves the functions  $X(\phi)$  plotted using analytic solutions for  $\mathcal{A}$  and  $\phi$ .

It worth to be noted that in Figs. 15 and 16 the arrows always show the direction of increasing scale factor.

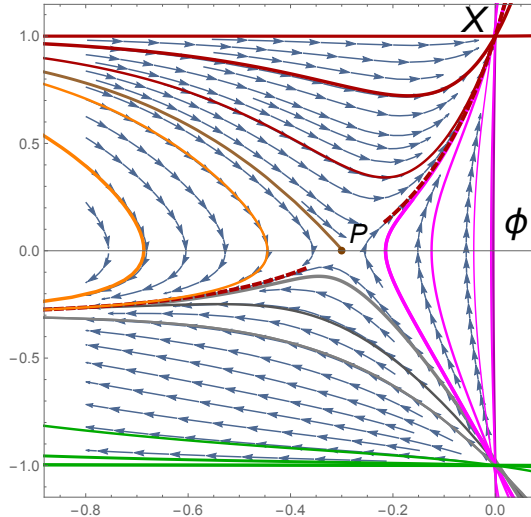


**Figure 16.** The behaviour of  $X(\phi)$  near the point  $P$  plotted using exact vacuum solutions and the stream of eq. (5.9) (blue lines). The legends are the same as in Fig. 15.

### 5.3 Non-vacuum RG flow

Now we turn our discussion to the finite-temperature case. In Sec. 4 we showed that non-zero temperature solutions are characterized by the parameter  $\alpha^1 \neq 0$ . This case is described by the additional variable  $Y$  defined through the blackening function (5.8). Here we deal with the system (5.4)-(5.5), which seems to be rather complicated comparing to the zero- $T$  case and one has to apply analytic solutions for  $\phi$  (5.12) and  $\mathcal{A}$  (5.19) with (3.5)-(3.9) to show the RG flow. The dynamical system (5.4)-(5.5) possesses critical points defined by the equation

$$Y = X^2 - 1. \quad (5.31)$$

In Fig. 17 these points are indicated by the red curve.

Let us first summarize results obtained in this section on one plot, see Fig. 17 where we show the flow in  $(X, Y)$  plane. Here:

- The left solutions defined for  $u < u_{02}$  start at  $u_{02} = 0$  at the point  $(X_{c1}, 0)$  on the  $(X, Y)$  plane, which is outside of the region bounded by the critical line. Then with decreasing  $u$  to  $u = u_s < 0$ , the functions  $X$  and  $Y$  reach infinities,  $X(u) \rightarrow -\infty$  and  $Y(u) \rightarrow -\infty$  for  $\alpha^1 > 0$  and  $Y(u) \rightarrow \infty$  for  $\alpha^1 < 0$ . Notice that we are interested in the case  $Y \geq 0$ . After the jump at  $u = u_s$  from  $-\infty$  to  $+\infty$ ,  $X(u)$  decreases from  $+\infty$  to a finite positive value at  $u \rightarrow -\infty$ , while  $Y(u)$  jumps from  $-\infty$  to  $\infty$  for  $\alpha^1 > 0$  (and from  $+\infty$  to  $-\infty$  for  $\alpha^1 < 0$ ), and after this jump it reaches a positive finite value at  $u \rightarrow -\infty$  for  $\alpha^1 > 0$  and a negative finite value for  $\alpha^1 < 0$ . For both cases the RG flow reaches the critical line at  $u = -\infty$  from the outside of the region bounded by the critical line.

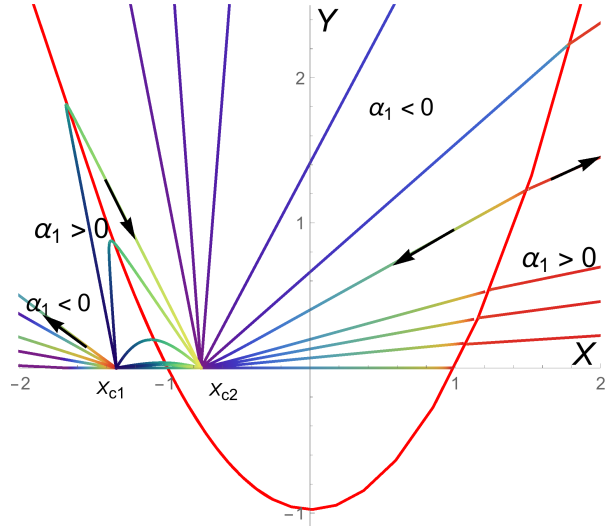


**Figure 17.** The RG flow in the  $(X, Y)$  plane for all analytical solutions governed by  $\sinh$ . Here arrows show increasing directions of  $\mathcal{A}$ , see Figs. 18-21. For  $Y = 0$  the direction of the flow is in accordance with direction of the vacuum flow presented in Fig. 15.  $C_1 = -C_2 = -2$ ,  $k = 0.4$ ,  $u_{01} = 1$ ,  $u_{02} = 0$ .

- The middle solutions start and end at fixed points  $(X_{c1}, 0)$  and  $(X_{c2}, 0)$ . They cross once the critical line at the points that correspond to zero of the potential, see Fig. 32 and an explanation below.
- The right branch solutions start at  $(X_{c2}, 0)$ . These solutions do not abandon the area bounded by the critical line, they stop on this line.

To see more clearly the behaviour of the RG flow at finite temperature it is useful to plot  $X$  and  $Y$  as functions of  $\phi$  for each of the analytical solution. Let us start from the left solutions. The characteristic feature of this solution are jumps that are realized at some points  $\phi_s$ . We have seen the jumps also for vacuum solutions, see Fig. 12A). Let us estimate the position of the point  $\phi_s$ , which corresponds to  $u = u_s$ , i.e.  $\phi_s = \phi(u_s)$ . At this point  $X$  and  $Y$  have infinite values and we note that in the system (5.4)-(5.5)  $\frac{3}{8} \left| \frac{d \log V}{d \phi} \right| < \infty$  and therefore near  $u = u_s$  the system takes the form

$$\frac{dX}{d\phi} \approx -\frac{4}{3} (1 - X^2 + Y), \quad (5.32)$$

$$\frac{dY}{d\phi} = -\frac{4}{3} (1 - X^2 + Y) \frac{Y}{X}, \quad (5.33)$$

so

$$\frac{dX}{dY} \approx \frac{X}{Y} \quad (5.34)$$

and

$$Y(u) = CX(u). \quad (5.35)$$

Plugging (5.35) in (5.32) we obtain

$$\frac{dX}{d\phi} \approx \frac{4}{3}X^2, \quad \Rightarrow X(\phi) = -\frac{3}{4(\phi - \phi_s)}. \quad (5.36)$$

In Fig. 18 **A**) and **B**) we plot the  $X$ -function using the "left" solutions (3.5) on  $\phi$  with different values of  $E_2$  and  $\alpha^1$  on both sides from the singular points  $\phi_s = \phi_s(E_2, \alpha^1)$ . We see again that in the non-vacuum case  $X$  can be positive as shown at **A**) and negative as shown at **B**). In Fig. 18 **C**) and **D**) we plot the  $Y$ -variable for the left solutions for both sides of the singular point  $\phi_s$ . We notice that to have  $Y$  function positive we take  $\alpha^1 < 0$  for  $\phi > \phi_s$  and  $\alpha^1 > 0$  for  $\phi < \phi_s$ . We also show the dependence of  $X$  and  $Y$  for the left solution on the energy scale  $\mathcal{A}$  in Figs. 18 **E**)-**H**). From Fig. 18**A**) we see that at  $\phi \rightarrow -\infty$

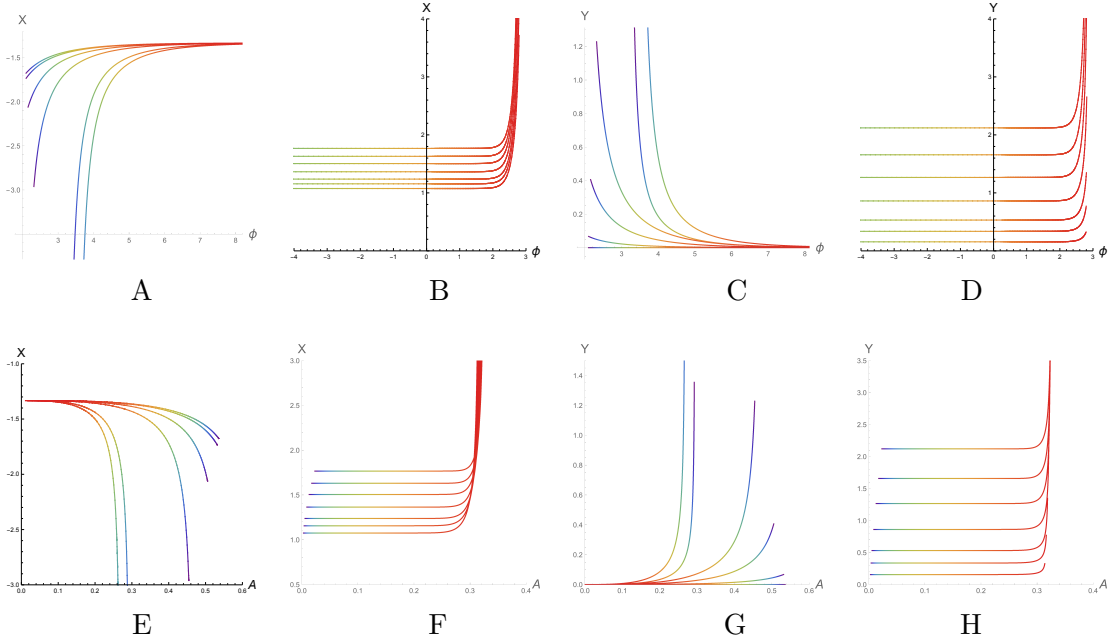


**Figure 18.** **Upper line:** A) and C) Non-vacuum solutions for  $X$  and  $Y$  on  $\phi$  built on the left solutions for  $\phi > \phi_s(E, \alpha^1)$ , here  $(E, \alpha^1) = (0.5, 0), (0.5, -0.1), (0.5, -0.5), (0.5, -1), (5, -0.5), (5, -1)$  from top to down; B) and D) the same solutions for  $X$  and  $Y$  for  $\phi < \phi_s(E, \alpha^1)$ , here  $E = 5, \alpha^1 = 0.075, 0.15, 0.22, 0.32, 0.42, 0.5, 0.58$  from top to down. **Bottom line:** the corresponding flows in the  $(\mathcal{A}, X)$  and  $(\mathcal{A}, Y)$  planes.

$X$  takes the constant value  $X_{c1}$ , however from Fig. 18**B**) we see that with  $\phi \rightarrow +\infty$   $X$  does to different constants, depending of the values of  $E, \alpha^1$ . In other words there are attractor points of  $X$  at some infinite values of  $\phi$ . To get the attractor points, we can assume that at this points with  $\phi \rightarrow \pm\infty$ :

$$X' = Y' = 0, \quad (5.37)$$

$$(1 - X^2 + Y) \neq 0. \quad (5.38)$$

Thus we have

$$\phi \rightarrow -\infty : 1 + \frac{3}{8X_{c2}}2k = 0 \Rightarrow X_{c2} = -\frac{3}{4}k, \quad (5.39)$$

$$\phi \rightarrow +\infty : 1 + \frac{3}{8X_{c1}}\frac{32}{9k} = 0 \Rightarrow X_{c1} = -\frac{4}{3k}. \quad (5.40)$$

that fit numerical data.

In Figs. 19 we present  $X$  and  $Y$  variables plotted using the middle analytical solutions with non-zero  $\alpha^1$  for  $\mathcal{A}$  and  $\phi$ . In Figs. 19 A) and C) we see that  $X$  is negative as for the corresponding vacuum case. The variable  $Y$  is positive for both dependences on  $\phi$  and  $\mathcal{A}$ , see in Fig. 19 B) and D), correspondingly. So the presence of the  $\alpha^1$  just slightly modifies the behaviour of the RG flow in this case. Finally, we come to the non-vacuum RG flow for

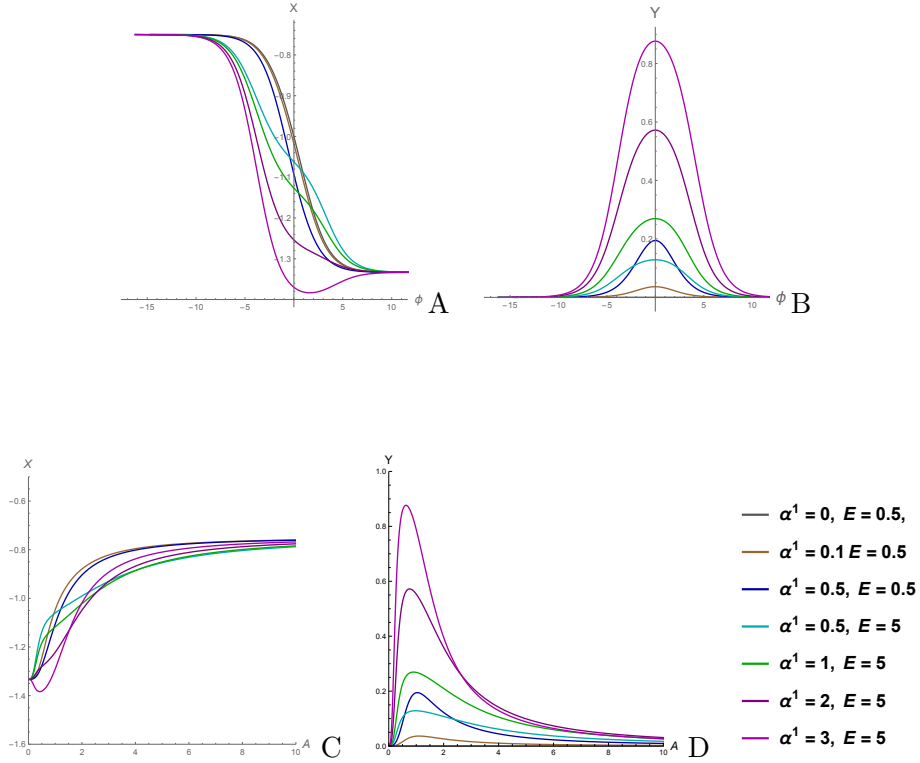


**Figure 19.** A) and B) show the dependence of  $X$  and  $Y$  on  $\phi$  at the middle solutions with  $\alpha^1 > 0$ ; C) and D) the RG flows in the  $(A, X)$  and  $(A, Y)$  planes at these solutions.  $C_1 = -C_2 = -2$ ,  $k = 0.4$  for all.

the right solutions with  $u > u_{01}$ . We remind the horizon of the black brane at  $u \rightarrow +\infty$  in this case is defined for  $\alpha^1 < 0$ . In Fig. 20 we draw  $X$  and  $Y$  as functions of  $\phi$  for different values of the negative  $\alpha^1$  and  $E_2$ . From Fig. 20A) we see that the behaviour of  $X$  can be changed by  $\alpha^1$  thus  $X$  becomes to be negative in the finite- $T$  case. At the same time for small values of  $\alpha^1$  it has the multivalued form as for the vacuum case. As for the  $Y$  function one can see from Fig. 20 B) that it is positive. In Fig. 21 we present the dependences of  $X$  and  $Y$  on the energy scale  $\mathcal{A}$ . We see that the behaviours of these variables remain.

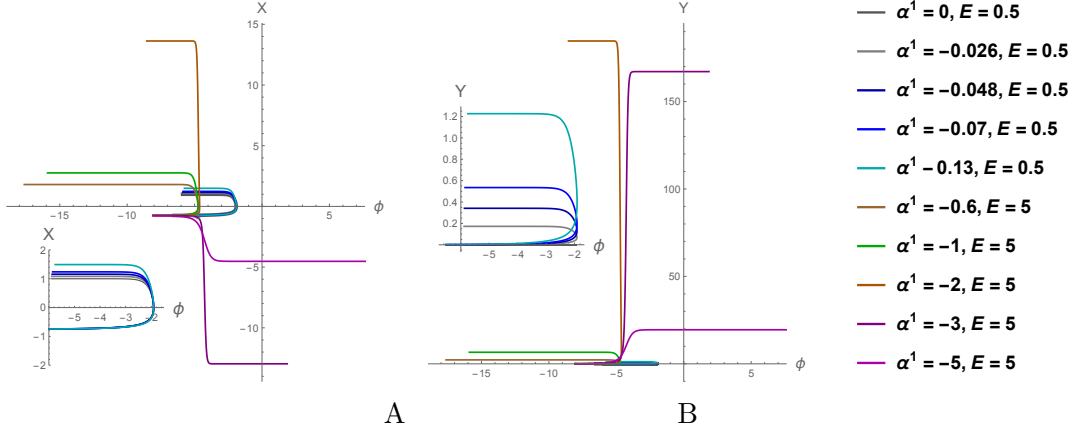


**Figure 20.** The dependence of  $X$  and  $Y$  on  $\phi$  for the right solution with  $\alpha^1 < 0$ . as an inset The inset are plots corresponding to small  $|\alpha^1|$ .  $C_1 = -C_2 = -2$ ,  $k = 0.4$ ,  $u_{01} = 1$ ,  $u_{02} = 0$ .

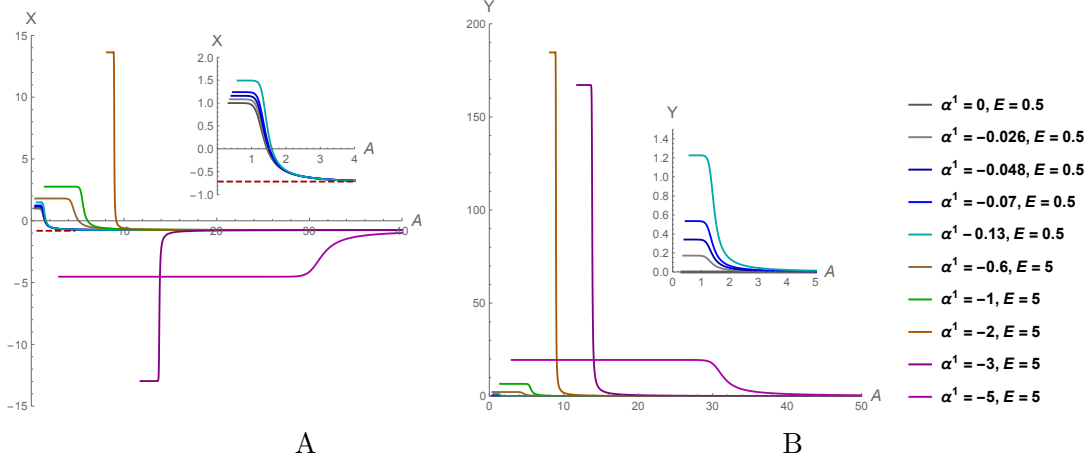


**Figure 21.** The RG flows for the right solution with  $\alpha^1 < 0$ . A) The flow in the  $(A, X)$  planes, B) The flow in the  $(A, Y)$  plane. The legends are the same for all plots and the in-plots are the plots corresponding to small  $|\alpha^1|$ .  $C_1 = -C_2 = -2$ ,  $k = 0.4$ ,  $u_{01} = 1$ ,  $u_{02} = 0$ .

#### 5.4 The running coupling $\lambda = e^\phi$ on the energy scale. Vacuum flow

It is important to know the behaviour of the running coupling  $\lambda = e^\phi$  on the energy scale  $A = \exp \mathcal{A}$ . One can trace this using the analytic solutions for  $\phi$  and  $\mathcal{A}$ . Both of them depend on the constant of integration  $E_1$ ,  $E_2$ ,  $\alpha^1$ ,  $u_{01}$ ,  $u_{02}$  and on the shape of the potential, which is defined by  $C_1$ ,  $C_2$  and  $k$ . We remind that  $E_1$ ,  $E_2$  and  $\alpha^1$  are not independent. In this subsection we consider  $\alpha^1 = 0$  case.

First let's take a look how the scale factor  $A = \exp \mathcal{A}$  depends on the dilaton. For this purpose we show in Fig. 22 the dependence of  $A$  on  $u$ . Next, we show in Fig. 23 the behaviour of the scalar factor  $A$  on the dilaton for three branches.

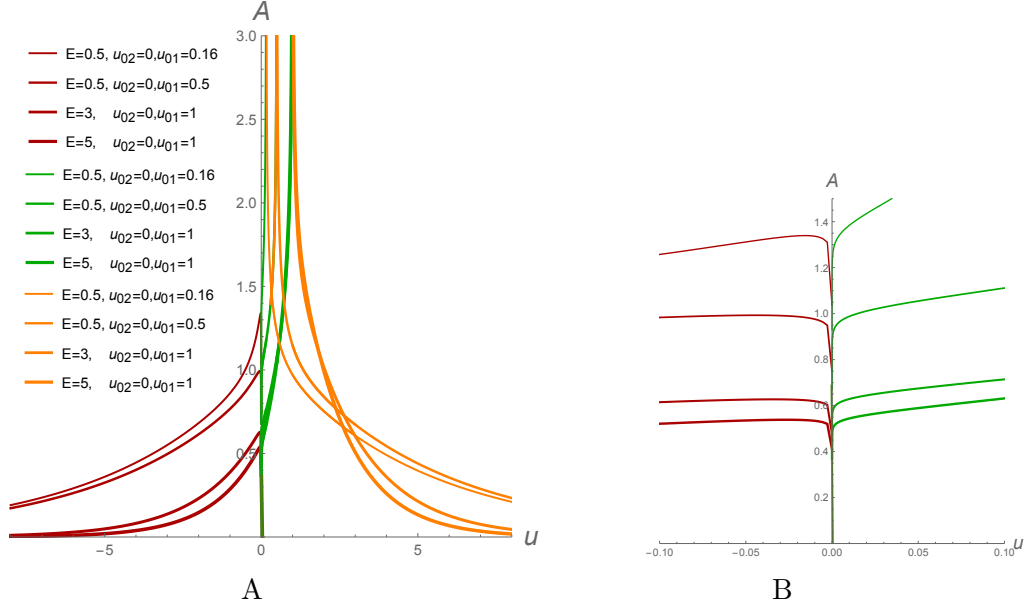


**Figure 22.** The behaviour of the scalar factor  $A$  at all 3 branches (the darker red curves for the left solution, the green ones for the middle and the orange ones for the right solution) and its zoom near  $u = 0$ . For all plots  $k = 0.4$ ,  $C_1 = -2$ ,  $C_2 = 2$ , different curves on the same plot correspond to the different values of  $|E_1| = |E_2|$ , labeled as  $E$  on the legends and different  $u_{01}$  and  $u_{01}$  also indicated on the legends.

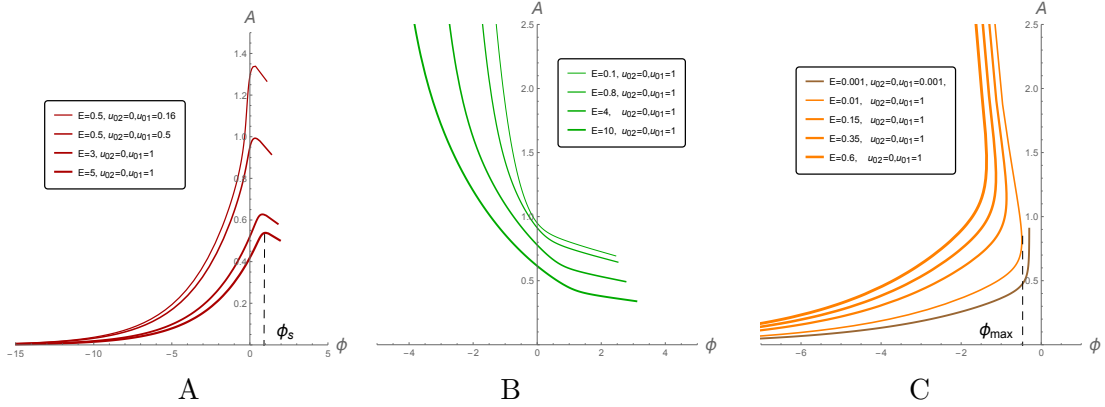


**Figure 23.** The behaviour of the scalar factor  $A$  on the dilaton plotted using the solutions for  $\mathcal{A}$  and  $\phi$ : A) the left branch with  $u_{02} > u$ , B) the middle branch  $u_{02} < u < u_{01}$ ; C) the right branch  $u > u_{01}$ . For all plots  $k = 0.4$ ,  $C_1 = -2$ ,  $C_2 = 2$ , different curves on the same plot correspond to the different values of  $|E_1| = |E_2|$ , labeled as  $E$  on the legends and different  $u_{01}$  and  $u_{01}$  also indicated on the legends.

We see that on left and middle solutions the dilaton interpolates between  $\pm\infty$  and for the right solution it starts at  $-\infty$  goes to the maximal value  $\phi_{max}$  and when goes back to

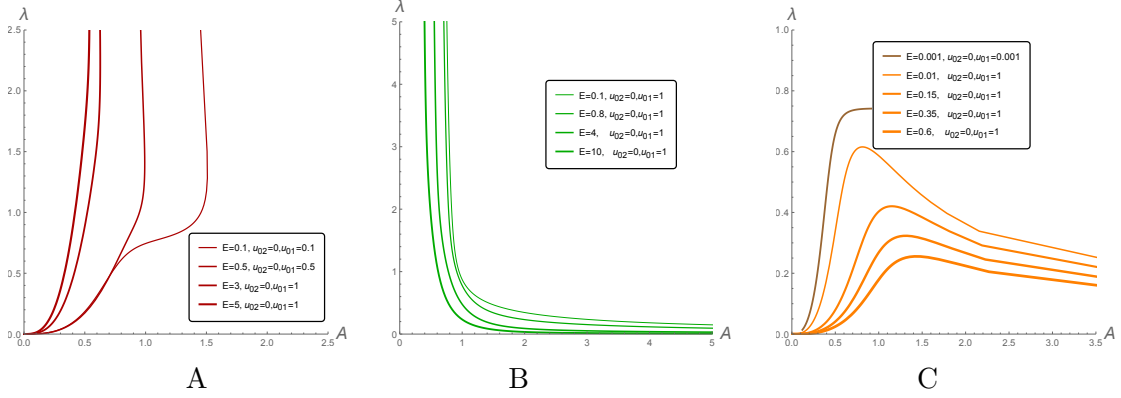


**Figure 24.** The dependence of the coupling constant on the scalar factor  $A$  on the dilaton plotted using the solutions for  $\mathcal{A}$  and  $\phi$ : A) the left branch with  $u_{02} > u$ , B) the middle branch  $u_{02} < u < u_{01}$ ; C) the right branch  $u > u_{01}$ . For all plots  $k = 0.4$ ,  $C_1 = -2$ ,  $C_2 = 2$ , different curves on the same plot correspond to the different values of  $|E_1| = |E_2|$ , labeled as  $E$  on the legends and different  $u_{01}$  and  $u_{02}$  also indicated on the legends.

$-\infty$  (we have seen this behaviour already in the previous sections). It is interesting, that in spite of that the dilaton has the similar behaviour on the left and middle solutions, the scale factor has rather different behavior on these solutions, namely, on the left solution when dilaton varies from  $-\infty$  to a special value  $\phi_s$ , the scalar factor increases, but after dilaton passes this special value  $\phi_s$ , the scale factor starts to decrease. For the middle solution when dilaton increases from  $-\infty$  to  $+\infty$ , the scale factor decreases from large positive values to zero. On the right solution the scale factor is not a monotonic function of the dilaton, for the dilaton varying from  $-\infty$  to the maximal possible value  $\phi_{max}$  the scale factor increases, and then dilaton decreases back to  $-\infty$  while the scalar factor increases to infinity.

In Fig. 24 the dependence of the coupling constant  $\lambda = \exp \phi$  on the scale factor  $A$  is presented for the zero-temperature solutions with (3.5)-(3.7). We get that

- as expected for solutions with  $u < u_{02}$ , see Fig. 24 A), where the dilaton tends to  $-\infty$  in the IR region and we have IR-free theory, while in the UV region the effective coupling  $\lambda \rightarrow +\infty$ .
- In Fig. 24 B) we see that the dependence of  $\lambda$  on  $A$  plotted on the middle solutions with  $u_{02} < u < u_{01}$  mimics the QCD behavior.
- The running coupling plotted as a function of the energy scale at Fig. 24 C) for the solutions with (3.7) shows that it is UV free as well as IR free theory, i.e. the running coupling has the form of the hill.

## 5.5 The running coupling $\lambda = e^\phi$ on the energy scale. Non-vacuum flow

### 5.5.1 Three branch solutions with $u_{01} \neq u_{02}$

Now let's see what happens with the behaviour of the running coupling on the energy scale at finite temperature. As we have seen before the temperature is related to the parameter  $\alpha^1$ . As in the previous section, Sect.5.4, to have an insight to possible behavior of the running coupling on the constructed solutions, we start with presenting the possible behavior of the scale factor as function of the domain wall coordinate  $u$  with (3.5)-(3.7) and then incorporated found in Sect. 4, see Fig. 9, behavior of the dilaton as function of  $u$ . It is worth to remind that the behavior of the dilaton as a function of  $u$  does not depend on the sign of  $\alpha^1$ , but as we will see in the moment, the scale factor depends on this sign.

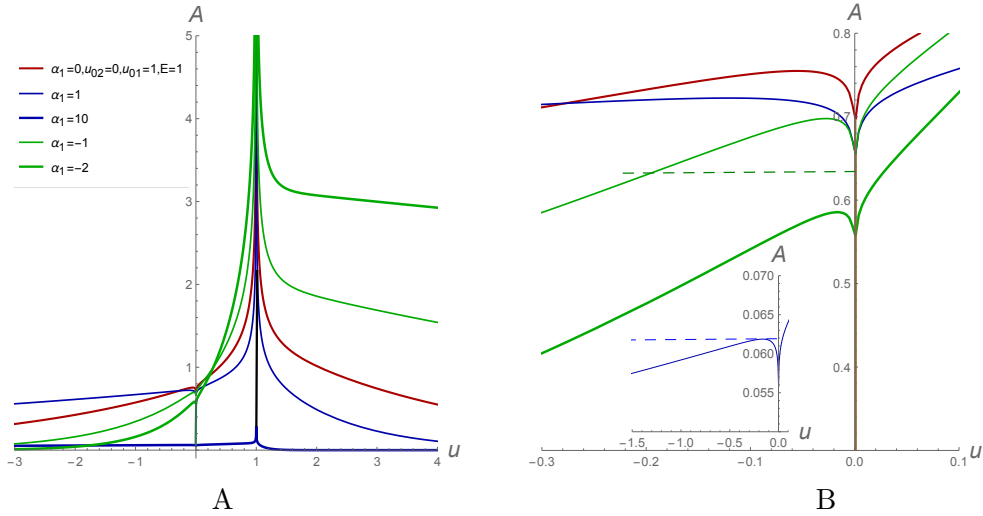


**Figure 25.** A. The dependence of the energy scale  $A = e^A$  on  $u$  at the left, middle and right solutions together. In all cases constants that define the potential are fixed and we vary  $\alpha^1$  as indicated at the legends. B. The zoom of the left solution near to  $u = 0$ .

In Fig. 25 we present the dependence of the scale factor  $A$  on  $u$  for the solution when  $u_{02} \neq u_{01}$ , (3.5)-(3.7) and different values of the parameter  $\alpha^1$ . Here the green curves correspond to negative  $\alpha^1$ , the darker red ones to  $\alpha^1 = 0$  and the blue curves to  $\alpha^1$  positive. Notice that the plots on Fig.25 correspond to  $u_{02} = 0$  and  $u_{01} > 0$ . We see that at the left branch all solutions describes at  $u \rightarrow -\infty$ , see Figs. 25.B. At the middle solutions the positive  $\alpha^1$  shifts  $A$  below, meanwhile the negative  $\alpha^1$  increases  $A$  near  $u_{01} > 0$  and decreases near  $u_{02} = 0$ . The positive  $\alpha^1$  decreases the factor  $A$ . At the right solution, for negative  $\alpha^1$  increasing  $|\alpha^1|$  we make the scale factor  $A$  faraway from zero and for positive  $\alpha^1$  decreasing  $|\alpha^1|$  we make the scale factor  $A$  closed to zero as compare to the vacuum case.

Since our black hole solutions require the negative  $\alpha^1$ , to make  $A$  close to zero at large  $u$  we can take both  $u_{01}$  and  $u_{02}$  negative, as we show in Fig.26. Here green line correspond to  $\alpha^1 < 0$ . We see that increasing  $|\alpha^1|$  we increase the scale factor at all branches. in Fig.26.B we see also that  $A \rightarrow 0$  at  $u \rightarrow \infty$ . We can support this behavior by few calculations.

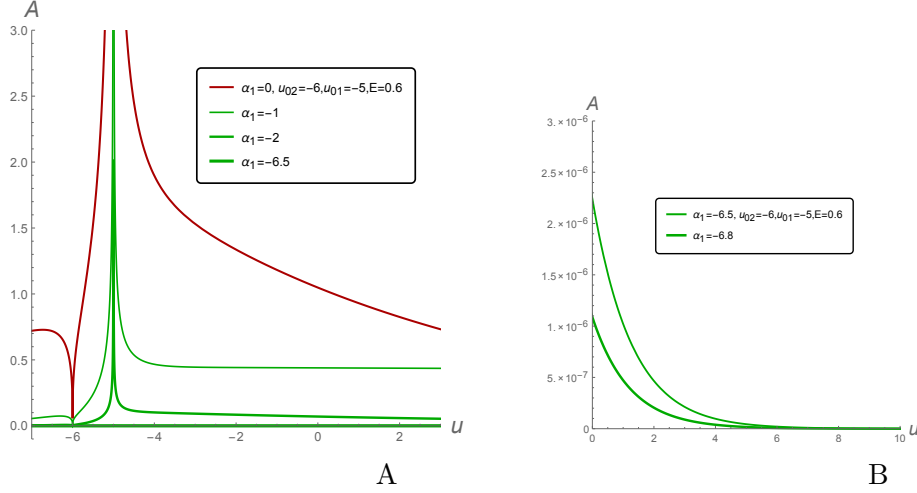


**Figure 26.** The plots show that for negative  $u_{01}$  and  $u_{02}$ , and negative  $\alpha^1$  at large  $u \rightarrow \infty$  the scale factor  $A$  decreases to be more closer to zero. The plot in the right panel zooms the area closed to zero of the left panel plot.

The asymptotics of  $\mathcal{A}$  given by (5.19) at  $u \rightarrow +\infty$  is

$$\mathcal{A}|_{u \rightarrow +\infty} = \frac{4\mu_1}{9k^2 - 16}(u - u_{01}) + \frac{9k^2\mu_2}{4(16 - 9k^2)}(u - u_{02}) - \frac{1}{3}\alpha^1 u \quad (5.41)$$

$$+ \frac{2}{9k^2 - 16} \log\left(\frac{C_1}{2E_1}\right) + \frac{9k^2}{8(16 - 9k^2)} \log\left(\frac{C_2}{2E_2}\right). \quad (5.42)$$

From (5.41) it is seen that  $\mathcal{A} \rightarrow -\infty$ , i.e. the scale factor  $A \rightarrow 0$ , with  $u \rightarrow +\infty$  if

$$\frac{4\mu_1}{9k^2 - 16} + \frac{9k^2\mu_2}{4(16 - 9k^2)} - \frac{1}{3}\alpha^1 < 0. \quad (5.43)$$

Plugging  $\mu_1$  and  $\mu_2$  into the latter equation one gets

$$\sqrt{\frac{8E_1}{3(9k^2 - 16)}} + \sqrt{\frac{3E_2}{2(16 - 9k^2)}} - \frac{1}{3}\alpha^1 < 0. \quad (5.44)$$

In the case of zero in the LHS of (5.44), i.e.

$$\frac{4\mu_1}{9k^2 - 16} + \frac{9k^2\mu_2}{4(16 - 9k^2)} - \frac{1}{3}\alpha^1 = 0, \quad (5.45)$$

the scale factor  $\mathcal{A}$  at infinity tends to the following constant value

$$\mathcal{A}|_{u \rightarrow +\infty} = -\frac{4\mu_1 u_{01}}{9k^2 - 16} - \frac{9k^2\mu_2 u_{02}}{4(16 - 9k^2)} + \frac{2}{9k^2 - 16} \log\left(\frac{C_1}{2E_1}\right) + \frac{9k^2}{8(16 - 9k^2)} \log\left(\frac{C_2}{2E_2}\right). \quad (5.46)$$

In Figs. 27 we show the solutions of the inequality (5.44). Here the white area shows the solutions to inequality (5.44), and the boundary shows the solution to (5.45). We see that when  $k \rightarrow 4/3$ , the area of validity of (5.44) shrinks to zero.

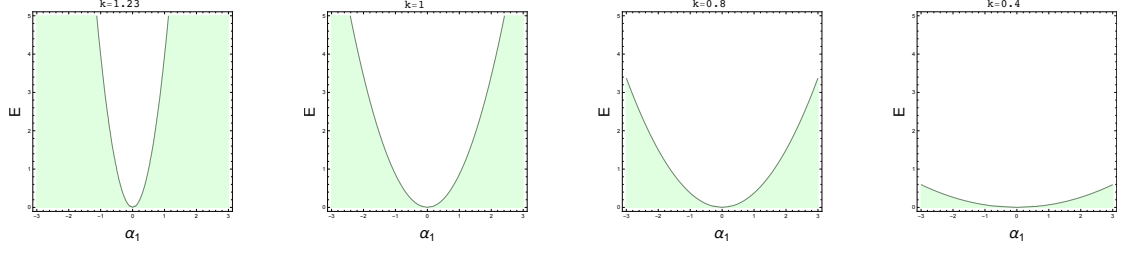


**Figure 27.** The white area show the solutions to inequality (5.44).

In Figs. 28 we present the parametric dependence of  $\lambda$  on  $A$  for the solution when  $u_{01} \neq u_{02}$ , (3.5)-(3.7), and different values of the parameter  $\alpha^1$ . (The upper line is for negative  $\alpha^1$  and the bottom one is for positive ones).

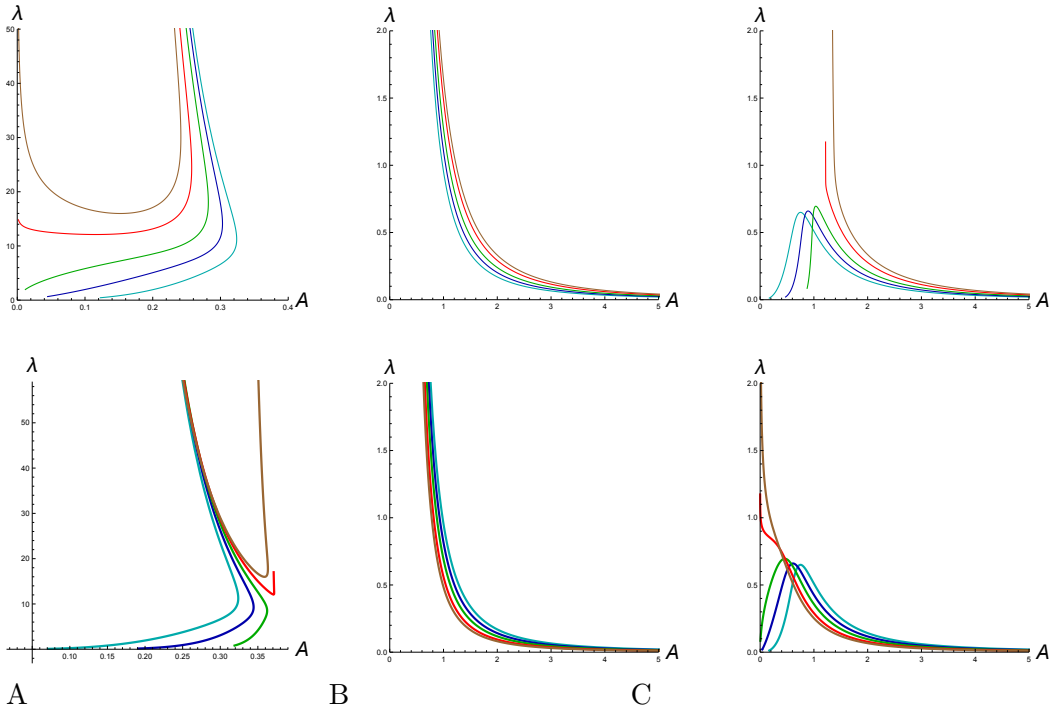


**Figure 28.** The dependence of  $\lambda$  on the energy scale  $A = e^A$  at the left solution A), the middle solution B), and the right one C). In all cases constants that fix the potential are fixed and we vary  $\alpha^1$ . Upper line:  $\alpha^1 = 0$  (cyan),  $\alpha^1 = -0.25$  (blue),  $\alpha^1 = -0.5$  (green),  $\alpha^1 = -0.8$  (red),  $\alpha^1 = -1$  (brown). Bottom line:  $\alpha^1 = 0$  (cyan),  $\alpha^1 = 0.25$  (blue),  $\alpha^1 = 0.5$  (green),  $\alpha^1 = 0.8$  (red),  $\alpha^1 = 1$  (brown). Double-values form for the left branch is related with the jumps, see Fig. 23 A).

These plots show the following behaviour.

- In Fig. 28 A) we show the dependence of  $\lambda$  on  $A$  for the left solution,  $u < u_{02}$ . We observe that the running coupling for this case is double-valued. The origin of the double-valued form is bounded from above of the factor  $A$  on the left solutions and its the hill form as a function on  $u$ , see Fig. 25 B). Moreover, the parameter  $\alpha^1$  affects essentially on the energy scale dependence of running coupling. For small negative  $\alpha^1$

the asymptotic regime with a large scale cannot be reached and at small scalar factor one get the IR freedom. But increasing  $|\alpha^1|$  keeping  $\alpha^1 < 0$  (curves above the red one at upper plot in Fig. 28 A)). For large positive  $\alpha^1$  we get the IR freedom, as to the UV behavior it seems non reachable at these solutions. The form of the dependence of the running coupling for the left solutions is far from that one for QCD.

- In Fig. 28 B) it is presented the behaviour of the running coupling for the middle solutions with  $u_{02} < u < u_{01}$ . We observe that the presence of the parameter  $\alpha^1$  and its sign can just slightly modify the behaviour of the coupling. One can say that in this picture we see reproducing of the running coupling for QCD. However, for the middle solutions only the vacuum case is well defined, as for the non-vacuum it seems not to be possible to construct a black brane with the horizon.

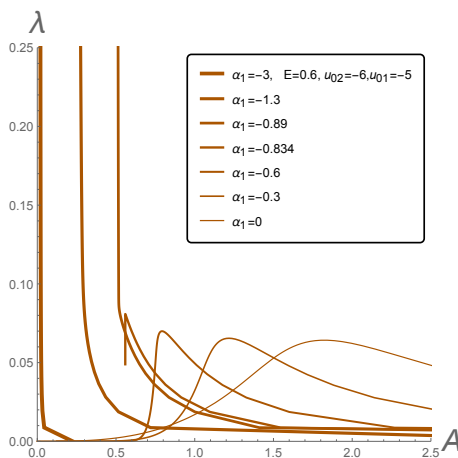


**Figure 29.** The dependence of  $\lambda$  on the energy scale  $A = e^A$  at the the right solution for negative  $u_{01}$  and  $u_{01}$  and negative  $\alpha^1$ , Here  $k = 1, C_1 = 1, C_2 = -3$ , all other parameters are indicated on the legend. We see the change of the regime near  $\alpha^1 = -0.834$ .

- Finally, in Fig. 28 C) we show the running coupling  $\lambda$  as a function of the energy scale  $A$  for the right solutions with  $u > u_{01}$ . We see that the IR dynamics can be changed by the appropriate values of  $\alpha^1$ . This comes from the fact the dilaton can change the asymptotics from  $-\infty$  to  $+\infty$  with  $\mu_1 > \mu_2$  as has been explained in Sect.4. If the chosen values of  $E_1, E_2, \alpha^1$  and  $k$  satisfy the inequality (5.44), than one can reach  $A \rightarrow 0$  and in this limit the coupling constant  $\lambda$  can go to 0 or to  $+\infty$ , depending the the chosen parameters. In particular, for parameter chosen as in Fig. 29, varying  $\alpha^1 < 0$  we change the IR regime: for small  $|\alpha^1| < |\alpha^c|$  we have the IR freedom and for  $|\alpha^1| > |\alpha^c|$  we get the increasing coupling constant in the IR regions. For  $A \rightarrow +\infty$  the running coupling  $\lambda$  goes to 0 for all chosen parameters providing the UV freedom. Or in others words, we can mimic the QCD RG flow for negative  $\alpha^1$  such that  $|\alpha^1| > |\alpha^c|$ .

### 5.5.2 Special case $u_{01} = u_{02}$

Now we turn to  $\lambda$  for the solutions  $u_{01} = u_{02}$ . In Fig. 30 we present the behaviour of the running coupling. We see that their behavior is similar to that one shown in Fig. 28 C). The presence of the parameter  $\alpha^1$  drastically changes the running coupling and one can observe  $\lambda \rightarrow +\infty$  at small values of the energy scale at finite temperature.

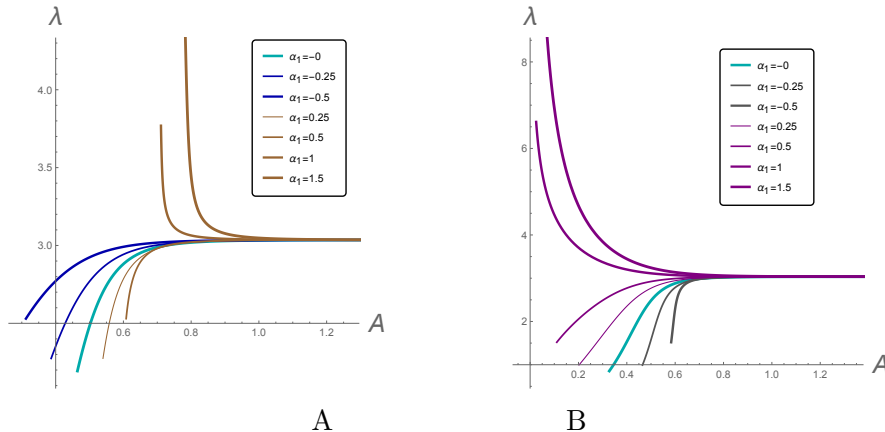


**Figure 30.** The behaviour  $\lambda = e^\phi$  on  $A = e^A$  on the left **A**) and right **B**) of the solutions (3.9) for different  $\alpha^1$  indicated at plots.

## 6 Conclusion and Discussion

We have presented some analytic solutions of Einstein equations coupled to a dilaton field, at zero and non-zero temperature, that correspond to holographic RG flows between different fixed points. The non-trivial form of the potential allows for a rich variety of different behaviors for the dilaton and the scale factor, corresponding to a coupling that can run to zero or to infinity in the UV and in the IR. In particular, we showed that the finite temperature solutions can behave very differently from the corresponding zero-temperature ones.

The next step in our program is to understand better these solutions from the point of view of the putative dual field theory, and to investigate possible applications of these solutions to the physics of QCD-like theories.

It would be interesting to determine the spectrum of fluctuations around these solutions, in particular the quasi-normal modes of the black brane solutions, and also to extend our ansatz in order to look for analytic time dependent solutions that describe out-of-equilibrium dynamics.

It would also be worthwhile to understand if the method we used, that reduces the Einstein equations to an integrable Toda chain, could be used for other case, for instance whether it is possible to relax the constraints (2.21)-(2.22) on the parameters of the potential, and in general achieve a classification of all cases that can be solved in this way. One way to approach this problem could be to reverse-engineer the dilaton potential and understand if it can come from some dimensional reduction.

It would also be interesting to consider the coupling of a Maxwell field in the bulk and find charged black hole solutions.

### **Acknowledgments**

GP would like to thank M. Jarvinen and E. Kiritsis for giving useful suggestions, and the Steklov Mathematical Institute for hospitality during the initial stages of this work. AG thanks Gleb Arutyunov, Eoin Ó Colgáin, Chanyong Park and Sunyoung Shin for useful conversations. AG is also very grateful for the warm hospitality DESY Theory Group, APCTP (Pohang) and Sogang University (Seoul).

## Appendix

### A The curvature invariants of the background

The ansatz for the metric is given by

$$ds^2 = -e^{2A(u)}dt^2 + e^{2B(u)}\sum_{i=1}^3 dy_i^2 + e^{2C(u)}du^2. \quad (\text{A.1})$$

The non-zero components of the Ricci tensor are

$$R_{00} = e^{2(A-C)} \left( (\dot{A})^2 + 3\dot{A}\dot{B} - \dot{A}\dot{C} + \ddot{A} \right), \quad (\text{A.2})$$

$$R_{11} = R_{22} = R_{33} = -e^{2(B-C)} \left( \dot{A}\dot{B} + 3\dot{B}^2 - \dot{B}\dot{C} + \dot{B} \right), \quad (\text{A.3})$$

$$R_{44} = -\dot{A}^2 - 3\dot{B}^2 + \left( \dot{A} + 3\dot{B} \right) \dot{C} - \ddot{A} - 3\ddot{B}. \quad (\text{A.4})$$

The scalar curvature reads

$$R = -2e^{-2C} \left[ \dot{A}^2 + 3\dot{A}\dot{B} + 6(\dot{B})^2 - \dot{A}\dot{C} - 3\dot{B}\dot{C} + \ddot{A} + 3\ddot{B} \right]. \quad (\text{A.5})$$

Thus, we have

$$\sqrt{|g|}R = -e^{A+3B-C} \left[ 2(\dot{A})^2 + 6\dot{A}\dot{B} + 12(\dot{B})^2 - 2\dot{A}\dot{C} - 6\dot{B}\dot{C} + 2\ddot{A} + 6\ddot{B} \right]. \quad (\text{A.6})$$

To find the solutions to the model we use the gauge  $C = A + 3B$  for (A.1). The generic form of the obtained solutions is

$$e^A = e^{A_1} e^{\alpha^1 u}, \quad e^B = e^{B_1} e^{-\frac{1}{3}\alpha^1 u}, \quad (\text{A.7})$$

where the functions  $A_1 = B_1$  and  $\alpha^1$  is a constant, which is equal to zero for the vacuum case. Now the scalar curvature (A.5) reads

$$R = -\frac{4}{3} \left( (\alpha^1)^2 - 9\dot{A}_1^2 + 6\ddot{A}_1 \right) e^{-8A_1}, \quad (\text{A.8})$$

that covers the vacuum case with  $\alpha^1 = 0$

$$R = \left( 12\dot{A}_1^2 - 8\ddot{A}_1 \right) e^{-8A_1}. \quad (\text{A.9})$$

The Kretschmann scalar is defined as follows

$$K = R_{abcd}R^{abcd}. \quad (\text{A.10})$$

Plugging the metric (A.1) we have

$$K = 4(\dot{A}^4 + 3\dot{A}^2\dot{B}^2 + 6\dot{B}^4 + 2\dot{A}^2\ddot{A} + 6\dot{B}^2\ddot{B} + (\dot{A}^2 + 3\dot{B}^2)\dot{C}^2 + \ddot{A}^2 + 3\ddot{B}^2 - 2(\dot{A}^3 + 3\dot{B}^3 + \dot{A}\ddot{A} + 3\dot{B}\ddot{B})\dot{C})e^{-4C}. \quad (\text{A.11})$$

One can write down the Kretschmann scalar of the non-vacuum solution ( $\alpha^1 \neq 0$ )

$$K = \frac{8}{27} \left( (\alpha^1 - 3\dot{A}_1)^2 (19\alpha^1 + 42\alpha^1 \dot{A}_1 + 63\dot{A}_1^2) + 36(\alpha^1 - 9\dot{A}_1^2)\ddot{A}_1 + 54\ddot{A}_1^2 \right) e^{-16A_1}. \quad (\text{A.12})$$

Taking into account that  $C = 4A_1$  and  $\alpha^1 = 0$  for the vacuum solution one obtains

$$K = 8(21\dot{A}_1^4 - 12\dot{A}_1^2\ddot{A}_1 + 2\ddot{A}_1^2)e^{-16A_1}. \quad (\text{A.13})$$

### A.1 The scalar curvature of the vacuum solutions.

Using the expression for the scalar curvature (A.9) and taking into account (2.43) and (2.48)-(2.49) one can write

$$\begin{aligned} R = & \frac{(C_1/2E_1)^{\frac{16}{16-9k^2}} (C_2/2E_2)^{\frac{-9k^2}{16-9k^2}}}{4(16-9k^2)^2} \left( 8(16-9k^2)(16\mu_1^2 - 9k^2\mu_2^2) + 128(9k^2-10)\mu_1^2 \coth(\mu_1(u-u_{01}))^2 \right. \\ & - 864k^2\mu_1\mu_2 \coth(\mu_1(u-u_{01})) \coth(\mu_2(u-u_{02})) \\ & \left. + 9k^2(128-45k^2)\mu_2^2 \coth(\mu_2(u-u_{02}))^2 \right) \sinh(\mu_1(u-u_{01}))^{\frac{32}{16-9k^2}} \sinh(\mu_2(u-u_{02}))^{\frac{-18k^2}{16-9k^2}}, \quad (\text{A.14}) \end{aligned}$$

It is exemplarily to look how the scalar curvature behaves for each branch of the solution.

- For the left solution which is defined for  $u < u_{02}$  we have the following limits

–  $u \rightarrow -\infty$ , so (A.14) can be rewritten as

$$R = \left( \frac{C_1}{2E_1} \right)^{\frac{16}{16-9k^2}} \left( \frac{C_2}{2E_2} \right)^{\frac{-9k^2}{16-9k^2}} \frac{3(16\mu_1 - 9k^2\mu_2)^2}{4(16-9k^2)^2} e^{-\frac{2(16\mu_1-9k^2\mu_2)}{16-9k^2}u}, \quad (\text{A.15})$$

The quantity  $(16\mu_1 - 9k^2\mu_2)$ , with  $\mu_1 = \sqrt{\left| \frac{3E_1}{2} \left( k^2 - \frac{16}{9} \right) \right|}$ ,  $\mu_2 = \sqrt{\left| \frac{3E_2}{2} \left( \left( \frac{16}{9} \right)^2 \frac{1}{k^2} - \frac{16}{9} \right) \right|}$ ,  $|E_1| = |E_2|$ ,  $0 < k < 4/3$  is always positive and the scalar curvature grows as  $u \rightarrow -\infty$ .

The scalar curvature in the conformal coordinates with  $z \rightarrow 0$

$$R = \left( \frac{C_1}{2E_1} \right)^{\frac{16}{16-9k^2}} \left( \frac{C_2}{2E_2} \right)^{\frac{-9k^2}{16-9k^2}} \frac{3(16\mu_1 - 9k^2\mu_2)^2}{4(16-9k^2)^2} \left( \frac{3\mu_1}{4+3k} z \right)^{-\frac{8}{3}}. \quad (\text{A.16})$$

- $u \rightarrow u_{02} - \epsilon$ , then the scalar curvature (A.14) takes the form

$$\begin{aligned} R = & \frac{(C_1/2E_1)^{\frac{16}{16-9k^2}} (C_2/2E_2)^{\frac{-9k^2}{16-9k^2}}}{4(16-9k^2)^2} \left( 8(16-9k^2)(16\mu_1^2 - 9k^2\mu_2^2) \right. \\ & + 128(9k^2-10)\mu_1^2 \coth(\mu_1(u_{02}-u_{01}))^2 - 864k^2\mu_1 \coth(\mu_1(u_{02}-u_{01}))(u-u_{02})^{-1} \\ & \left. + 9k^2(128-45k^2)(u-u_{02})^{-2} \right) \sinh(\mu_1(u_{02}-u_{01}))^{\frac{32}{16-9k^2}} (\mu_2(u-u_{02}))^{\frac{-18k^2}{16-9k^2}}, \quad (\text{A.17}) \end{aligned}$$

where one can see that the scalar curvature (A.17) has divergencies. In the conformal coordinates the scalar curvature at  $u \rightarrow u_02 - \epsilon$  is

$$\begin{aligned}
R = & \frac{(C_1/2E_1)^{\frac{16}{16-9k^2}} (C_2/2E_2)^{\frac{-9k^2}{16-9k^2}}}{4(16-9k^2)^2} \left( 8(16-9k^2)(16\mu_1^2 - 9k^2\mu_2^2) \right. \\
& + 128(9k^2 - 10)\mu_1^2 \coth(\mu_1(u_{02} - u_{01}))^2 - 864k^2\mu_1 \coth(\mu_1(u_{02} - u_{01}))(u - u_{02})^{-1} \\
& \left. + 9k^2(128 - 45k^2)(u - u_{02})^{-2} \right) \sinh(\mu_1(u_{02} - u_{01}))^{\frac{32}{16-9k^2}} \left( \mu_2 \frac{4(16-9k^2)}{64-9k^2} z \right)^{\frac{-72k^2}{64-9k^2}}.
\end{aligned} \tag{A.18}$$

- The middle solution with  $u \in (u_{01}; u_{02})$  can be characterized by the following limits

–  $u \rightarrow u_{02} + \epsilon$  with

$$\begin{aligned}
R = & \frac{(C_1/2E_1)^{\frac{16}{16-9k^2}} (C_2/2E_2)^{\frac{-9k^2}{16-9k^2}}}{4(16-9k^2)^2} \left( 8(16-9k^2)(16\mu_1^2 - 9k^2\mu_2^2) \right. \\
& + 128(9k^2 - 10)\mu_1^2 \coth(\mu_1(u_{02} - u_{01}))^2 - 864k^2\mu_1 \coth(\mu_1(u_{02} - u_{01}))(u - u_{02})^{-1} \\
& \left. + 9k^2(128 - 45k^2)(u - u_{02})^{-2} \right) \sinh(\mu_1(u_{02} - u_{01}))^{\frac{32}{16-9k^2}} (\mu_2(u - u_{02}))^{\frac{-18k^2}{16-9k^2}}.
\end{aligned} \tag{A.19}$$

which has the same divergencies as (A.17) for the left solution. In the conformal coordinates the scalar curvature (A.19) is the same as (A.18).

–  $u \rightarrow u_{01} - \epsilon$ , so (A.14) reads as

$$\begin{aligned}
R = & \frac{(C_1/2E_1)^{\frac{16}{16-9k^2}} (\sqrt{C_2/2E_2} \sinh(\mu_2(u_{01} - u_{02})))^{\frac{-18k^2}{16-9k^2}}}{4(16-9k^2)^2} \left( 8(16-9k^2)(16\mu_1^2 - 9k^2\mu_2^2) \right. \\
& + 128(9k^2 - 10)(u_{01} - u)^{-2} - 864k^2\mu_2(u_{01} - u)^{-1} \coth(\mu_2(u_{01} - u_{02})) \\
& \left. + 9k^2(128 - 45k^2)\mu_2^2 \coth(\mu_2(u_{01} - u_{02}))^2 \right) (\mu_1(u_{01} - u))^{\frac{32}{16-9k^2}},
\end{aligned} \tag{A.20}$$

that is regular. As for the scalar curvature written in the conformal coordinates

$$\begin{aligned}
R = & \frac{(C_1/2E_1)^{\frac{16}{16-9k^2}} (\sqrt{C_2/2E_2} \sinh(\mu_2(u_{01} - u_{02})))^{\frac{-18k^2}{16-9k^2}}}{4(16-9k^2)^2} \left( 8(16-9k^2)(16\mu_1^2 - 9k^2\mu_2^2) \right. \\
& + 128(9k^2 - 10)(u_{01} - u)^{-2} - 864k^2\mu_2(u_{01} - u)^{-1} \coth(\mu_2(u_{01} - u_{02})) \\
& \left. + 9k^2(128 - 45k^2)\mu_2^2 \coth(\mu_2(u_{01} - u_{02}))^2 \right) \left( \mu_1 \frac{9k^2 - 4}{16 - 9k^2} z \right)^{\frac{32}{4-9k^2}},
\end{aligned} \tag{A.21}$$

where  $z \rightarrow +\infty$  and  $k$  should be greater then  $\frac{2}{3}$ .

- For the right solution with  $u > u_{01}$  one has

–  $u \rightarrow u_{01} + \epsilon$

$$R = \frac{(C_1/2E_1)^{\frac{16}{16-9k^2}} (\sqrt{C_2/2E_2} \sinh(\mu_2(u_{01} - u_{02})))^{\frac{-18k^2}{16-9k^2}}}{4(16-9k^2)^2} \left( 8(16-9k^2)(16\mu_1^2 - 9k^2\mu_2^2) \right. \\ \left. + 128(9k^2 - 10)(u - u_{01})^{-2} - 864k^2\mu_2(u - u_{01})^{-1} \coth(\mu_2(u_{01} - u_{02})) \right. \\ \left. + 9k^2(128 - 45k^2)\mu_2^2 \coth(\mu_2(u_{01} - u_{02}))^2 \right) (\mu_1(u - u_{01}))^{\frac{32}{16-9k^2}}, \quad (\text{A.22})$$

The scalar curvature in the conformal coordinates matches with (A.21).

– For the right solution with  $u > u_{01}$  one has

–  $u \rightarrow +\infty$

$$R = \left( \frac{C_1}{2E_1} \right)^{\frac{16}{16-9k^2}} \left( \frac{C_2}{2E_2} \right)^{-\frac{9k^2}{16-9k^2}} \frac{3(16\mu_1 - 9k^2\mu_2)^2}{4(16-9k^2)^2} e^{\frac{2(16\mu_1 - 9k^2\mu_2)}{16-9k^2}u}. \quad (\text{A.23})$$

As for the left solution the scalar curvature (A.22) grows due to  $(16\mu_1 - 9k^2\mu_2) > 0$  as for (A.15) with  $u \rightarrow -\infty$ . In the conformal coordinates

$$R = \left( \frac{C_1}{2E_1} \right)^{\frac{16}{16-9k^2}} \left( \frac{C_2}{2E_2} \right)^{-\frac{9k^2}{16-9k^2}} \frac{3(16\mu_1 - 9k^2\mu_2)^2}{4(16-9k^2)^2} \left( \frac{3\mu_1}{4+3k}z \right)^{-\frac{8}{3}}. \quad (\text{A.24})$$

with  $z \rightarrow 0$ .

• Let's find the scalar curvature for the special case of the solution with  $u_{01} = u_{02} = u_0$ .

The general formula for the scalar curvature with  $u_{01} = u_{02} = u_0$  reads

$$R = \frac{(\sqrt{\frac{C_1}{2E_1}} \sinh(\mu_1(u - u_{01})))^{\frac{32}{16-9k^2}} (\sqrt{\frac{C_2}{2E_2}} \sinh(\mu_2(u - u_{01})))^{\frac{-18k^2}{-16+9k^2}}}{4(16-9k^2)^2} \cdot \left( 8(9k^2 - 16)(9k^2\mu_2^2 - 16\mu_1^2) \right. \\ \left. + 128(-10 + 9k^2)\mu_1^2 \coth^2(\mu_1 u) - 864k^2\mu_1\mu_2 \coth(\mu_1 u) \coth(\mu_2 u) \right. \\ \left. + 9k^2(128 - 45k^2)\mu_2^2 \coth^2(\mu_2 u) \right). \quad (\text{A.25})$$

Here one has to study the behaviour of the scalar curvature in the limits of small  $u$  and  $u \rightarrow +\infty$ .

For  $u \rightarrow 0$  one has

$$R = -\frac{5}{4} \left( \sqrt{\frac{C_1}{2E_1}} \mu_1 \right)^{\frac{32}{16-9k^2}} \left( \sqrt{\frac{C_2}{2E_2}} \mu_2 \right)^{\frac{18k^2}{9k^2-16}}. \quad (\text{A.26})$$

So, one comes to a background with the constant negative curvature in the case of small values of  $u$ .

For  $u \rightarrow +\infty$  we obtain

$$R = \frac{3}{4} \frac{(16\mu_1 - 9k^2\mu_2)^2}{(16-9k^2)^2} \left( \frac{C_1}{2E_1} \right)^{\frac{32}{16-9k^2}} \left( \frac{C_2}{2E_2} \right)^{-\frac{18k^2}{-16+9k^2}} e^{\frac{2(16\mu_1 - 9k^2\mu_2)}{16-9k^2}u}, \quad (\text{A.27})$$

that is an agreement with (A.23). The corresponding expression in the scalar coordinates matches with (A.36).

## A.2 The scalar curvature of the non-vacuum solutions.

Now we turn to the non-vacuum background (4.1) with (4.3)-(4.5), which is characterized by a non-zero parameter  $\alpha^1$ . The scalar curvature for the non-vacuum case reads

$$\begin{aligned}
R = & -\left(8(9k^2 - 16)\left(\frac{2}{3}(\alpha^1)^2(9k^2 - 16) + 16\mu_1^2 - 9k^2\mu_2^2\right) + 128(10 - 9k^2)\mu_1^2 \coth(\mu_1(u - u_{01}))^2\right. \\
& \left. - 864k^2\mu_1\mu_2 \coth(\mu_1(u - u_{01})) \coth(\mu_2(u - u_{02})) + 9k^2(-128 + 45k^2)\mu_2^2 \coth^2(\mu_2(u - u_{02}))\right) \\
& \cdot \frac{\left(\sqrt{\frac{C_1}{2E_1}} \sinh(\mu_1(u - u_{01}))\right)^{\frac{32}{16-9k^2}} \left(\sqrt{\frac{C_2}{2E_2}} \sinh(\mu_2(u - u_{02}))\right)^{\frac{18k^2}{9k^2-16}}}{4(16 - 9k^2)^2}. \tag{A.28}
\end{aligned}$$

As for the vacuum solution it is instructive to see the scalar curvature for each of the branches with certain limits.

- The left solution with  $u < u_{02}$  has the following scalar curvature

–  $u \rightarrow -\infty$  one has

$$R = \left(\frac{C_1}{2E_1}\right)^{\frac{16}{16-9k^2}} \left(\frac{C_2}{2E_2}\right)^{-\frac{9k^2}{16-9k^2}} \left(\frac{3(16\mu_1 - 9k^2\mu_2)^2}{4(16 - 9k^2)^2} - \frac{4}{3}(\alpha^1)^2\right) e^{-\frac{2(16\mu_1 - 9k^2\mu_2)}{16-9k^2}u}. \tag{A.29}$$

In the conformal coordinates with  $z \rightarrow 0$  the curvature (A.29) can be rewritten as

$$R = \left(\frac{C_1}{2E_1}\right)^{\frac{16}{16-9k^2}} \left(\frac{C_2}{2E_2}\right)^{-\frac{9k^2}{16-9k^2}} \left(\frac{3(16\mu_1 - 9k^2\mu_2)^2}{4(16 - 9k^2)^2} - \frac{4}{3}(\alpha^1)^2\right) \left(\frac{\tilde{A}}{C}z\right)^{\frac{2(16\mu_1 - 9k^2\mu_2)}{16-9k^2}}, \tag{A.30}$$

– for the limit  $u \rightarrow u_{02} - \epsilon$

$$\begin{aligned}
R = & -\left(8(9k^2 - 16)\left(\frac{2}{3}(\alpha^1)^2(9k^2 - 16) + 16\mu_1^2 - 9k^2\mu_2^2\right)\right. \\
& \left. + 128(10 - 9k^2)\mu_1^2 \coth(\mu_1(u_{01} - u_{02}))^2\right. \\
& \left. - 864k^2\mu_1 \coth(\mu_1(u_{01} - u_{02}))(u - u_{02})^{-1} + 9k^2(-128 + 45k^2)(u - u_{02})^{-2}\right) \\
& \cdot \frac{\left(\sqrt{\frac{C_1}{2E_1}} \sinh(\mu_1(u_{01} - u_{02}))\right)^{\frac{32}{16-9k^2}} \left(\sqrt{\frac{C_2}{2E_2}} \mu_2(u - u_{02})\right)^{\frac{18k^2}{9k^2-16}}}{4(16 - 9k^2)^2}. \tag{A.31}
\end{aligned}$$

as for the vacuum case (A.17) the scalar curvature is divergent at  $u_{02}$ .

In the conformal coordinates (A.31) reads

$$\begin{aligned}
R = & -\left(8(9k^2 - 16)\left(\frac{2}{3}(\alpha^1)^2(9k^2 - 16) + 16\mu_1^2 - 9k^2\mu_2^2\right)\right. \\
& + 128(10 - 9k^2)\mu_1^2 \coth(\mu_1(u_{01} - u_{02}))^2 \\
& - 864k^2\mu_1 \coth(\mu_1(u_{01} - u_{02}))(u - u_{02})^{-1} + 9k^2(-128 + 45k^2)(u - u_{02})^{-2}) \\
& \cdot \frac{\left(\sqrt{\frac{C_1}{2E_1}} \sinh(\mu_1(u_{01} - u_{02}))\right)^{\frac{32}{16-9k^2}} \left(\sqrt{\frac{C_2}{2E_2}} \mu_2 \frac{4(16-9k^2)}{64-9k^2} z\right)^{\frac{-72k^2}{64-9k^2}}}{4(16 - 9k^2)^2}. \tag{A.32}
\end{aligned}$$

- The middle solution defined for  $u \in (u_{01}; u_{02})$ .

- For  $u \rightarrow u_{02} + \epsilon$  the scalar curvature matches with the curvature given by (A.31). As well as in the conformal coordinates it is the same as (A.32).

One can see that scalar curvature of the middle solution in the non-vacuum case has also a singularity at  $u_{01}$ .

- $u \rightarrow u_{01} - \epsilon$

$$\begin{aligned}
R = & -\left(8(9k^2 - 16)\left(\frac{2}{3}(\alpha^1)^2(9k^2 - 16) + 16\mu_1^2 - 9k^2\mu_2^2\right) + 128(10 - 9k^2)(u - u_{01})^{-2}\right. \\
& - 864k^2\mu_2(u - u_{01})^{-1} \coth(\mu_2(u_{01} - u_{02})) + 9k^2(-128 + 45k^2)\mu_2^2 \coth^2(\mu_2(u_{01} - u_{02}))\left.)\right) \\
& \cdot \frac{\left(\sqrt{\frac{C_1}{2E_1}} \mu_1(u - u_{01})\right)^{\frac{32}{16-9k^2}} \left(\sqrt{\frac{C_2}{2E_2}} \sinh(\mu_2(u_{01} - u_{02}))\right)^{\frac{18k^2}{9k^2-16}}}{4(16 - 9k^2)^2}. \tag{A.33}
\end{aligned}$$

or in the conformal coordinates with  $z \rightarrow +\infty$

$$\begin{aligned}
R = & -\left(8(9k^2 - 16)\left(\frac{2}{3}(\alpha^1)^2(9k^2 - 16) + 16\mu_1^2 - 9k^2\mu_2^2\right) + 128(10 - 9k^2)(u - u_{01})^{-2}\right. \\
& - 864k^2\mu_2(u - u_{01})^{-1} \coth(\mu_2(u_{01} - u_{02})) + 9k^2(-128 + 45k^2)\mu_2^2 \coth^2(\mu_2(u_{01} - u_{02}))\left.)\right) \\
& \cdot \frac{\left(\sqrt{\frac{C_1}{2E_1}} \mu_1 \frac{9k^2-4}{16-9k^2}\right)^{\frac{32}{4-9k^2}} \left(\sqrt{\frac{C_2}{2E_2}} \sinh(\mu_2(u_{01} - u_{02}))\right)^{\frac{18k^2}{9k^2-16}}}{4(16 - 9k^2)^2}. \tag{A.34}
\end{aligned}$$

- The right solution with  $u > u_{01}$

- $u \rightarrow u_{01} + \epsilon$

$$\begin{aligned}
R = & -\left(8(9k^2 - 16)\left(\frac{2}{3}(\alpha^1)^2(9k^2 - 16) + 16\mu_1^2 - 9k^2\mu_2^2\right) + 128(10 - 9k^2)(u - u_{01})^{-2}\right. \\
& - 864k^2\mu_2(u - u_{01})^{-1} \coth(\mu_2(u_{01} - u_{02})) + 9k^2(-128 + 45k^2)\mu_2^2 \coth^2(\mu_2(u_{01} - u_{02}))\left.)\right) \\
& \cdot \frac{\left(\sqrt{\frac{C_1}{2E_1}} \mu_1(u - u_{01})\right)^{\frac{32}{16-9k^2}} \left(\sqrt{\frac{C_2}{2E_2}} \sinh(\mu_2(u_{01} - u_{02}))\right)^{\frac{18k^2}{9k^2-16}}}{4(16 - 9k^2)^2}. \tag{A.35}
\end{aligned}$$

The scalar curvature in the conformal coordinates coincides with (A.34).

–  $u \rightarrow +\infty$

$$R = \left( \frac{C_1}{2E_1} \right)^{\frac{16}{16-9k^2}} \left( \frac{C_2}{2E_2} \right)^{-\frac{9k^2}{16-9k^2}} \left( \frac{3(16\mu_1 - 9k^2\mu_2)^2}{4(16-9k^2)^2} - \frac{4}{3}(\alpha^1)^2 \right) e^{\frac{2(16\mu_1-9k^2\mu_2)}{16-9k^2}u}. \quad (\text{A.36})$$

The curvature (A.36) can be presented in the conformal coordinates as

$$R = \left( \frac{C_1}{2E_1} \right)^{\frac{16}{16-9k^2}} \left( \frac{C_2}{2E_2} \right)^{-\frac{9k^2}{16-9k^2}} \left( \frac{3(16\mu_1 - 9k^2\mu_2)^2}{4(16-9k^2)^2} - \frac{4}{3}(\alpha^1)^2 \right) \left( \frac{\tilde{A}}{C} z \right)^{\frac{2(16\mu_1-9k^2\mu_2)}{16-9k^2}}, \quad (\text{A.37})$$

where the conformal coordinate  $z$  is given by (4.11) with  $\tilde{A}$  (4.12).

It should be noted that the scalar curvatures given by (A.29) and (A.36) can be equal to zero if the parameter  $\alpha^1$  is taken as

$$\alpha^1 = \pm \sqrt{\frac{(16-9k^2)E_2}{6k^2}}. \quad (\text{A.38})$$

### A.3 The Kretschmann scalar for the solution with $u > u_{01}$

For the vacuum solution defined for  $u > u_{01}$  (the right solution) with  $u \rightarrow u_{01} + \epsilon$  one has

$$K \sim k_0(u - u_{01})^{\frac{64}{16-9k^2}} \sum_{i=0}^4 c_i (u - u_{01})^{-i}, \quad (\text{A.39})$$

where  $k_0$  and  $c_i$   $i = 0, \dots, 4$  are some constants.

As for  $u \rightarrow +\infty$  the Kretschmann scalar for the right solution with (2.48)-(2.49) takes the form

$$K = \frac{21(16\mu_1 - 9k^2\mu_2)^4}{32(16-9k^2)^4} \left( \frac{C_1}{2E_1} \right)^{\frac{32}{16-9k^2}} \left( \frac{C_2}{2E_2} \right)^{\frac{18k^2}{9k^2-16}} e^{\frac{4(16\mu_1-9k^2\mu_2)}{16-9k^2}u}. \quad (\text{A.40})$$

$u \rightarrow u_{01} + \epsilon$

$$K \sim k_0(u - u_{01})^{\frac{64}{16-9k^2}} \sum_{i=0}^4 c_i (\#(\alpha^1)^i) (u - u_{01})^{-i}, \quad (\text{A.41})$$

$$(\text{A.42})$$

$u \rightarrow +\infty$

$$K = \frac{(4\alpha^1(9k^2 - 16) + 27k^2\mu_2 - 48\mu_1)^2}{864(16-9k^2)^4} \left( \frac{C_1}{2E_1} \right)^{\frac{32}{16-9k^2}} \left( \frac{C_2}{2E_2} \right)^{\frac{18k^2}{9k^2-16}} e^{\frac{4(16\mu_1-9k^2\mu_2)}{16-9k^2}u} \cdot (304(\alpha^1)^2(16-9k^2)^2 + 168\alpha^1(9k^2-16)(16\mu_1-9k^2\mu_2) + 63(16\mu_1-9k^2\mu_2)^2) \quad (\text{A.43})$$

## B The scalar field

We have the following relation for the scalar field

$$(\partial\varphi)^2 = e^{-2C} \left( \frac{\partial\phi}{\partial u} \right)^2. \quad (\text{B.1})$$

The dilaton solution defined for  $u > u_{01}$  reads

$$\phi = \frac{9k}{9k^2 - 16} \log \left( \sqrt{\frac{C_2}{C_1}} \frac{\sinh(\mu_2(u - u_{02}))}{\sinh(\mu_1(u - u_{01}))} \right). \quad (\text{B.2})$$

The derivative of the dilaton with respect to  $u$ -variable is

$$\frac{\partial\phi}{\partial u} = \frac{9k}{9k^2 - 16} \left( -\mu_1 \frac{\cosh(\mu_1(u - u_{01}))}{\sinh(\mu_1(u - u_{01}))} + \mu_2 \frac{\cosh(\mu_2(u - u_{02}))}{\sinh(\mu_2(u - u_{02}))} \right), \quad (\text{B.3})$$

$$\left( \frac{\partial\phi}{\partial u} \right)^2 = \frac{81k^2}{(16 - 9k^2)^2} (\mu_1 \coth(\mu_1(u - u_{01})) - \mu_2 \coth(\mu_2(u - u_{02})))^2. \quad (\text{B.4})$$

For the vacuum case one has

$$e^{-2C} = \left( \sqrt{\frac{C_1}{2E_1}} \sinh(\mu_1(u - u_{01})) \right)^{\frac{32}{16-9k^2}} \left( \sqrt{\frac{C_2}{2E_2}} \sinh(\mu_2(u - u_{02})) \right)^{\frac{18k^2}{9k^2-16}}. \quad (\text{B.5})$$

The dilaton for  $u \rightarrow u_{01} + \epsilon$  reads

$$\begin{aligned} (\partial\varphi)^2 &= \frac{81k^2}{(16 - 9k^2)^2} ((u - u_{01})^{-1} - \mu_2 \coth(\mu_2(u_{01} - u_{02})))^2 \\ &\cdot \left( \sqrt{\frac{C_1}{2E_1}} \mu_1(u - u_{01}) \right)^{\frac{32}{16-9k^2}} \left( \sqrt{\frac{C_2}{2E_2}} \sinh(\mu_2(u_{01} - u_{02})) \right)^{\frac{18k^2}{9k^2-16}}. \end{aligned} \quad (\text{B.6})$$

Since  $0 < k < 4/3$  the quantity  $(\partial\varphi)^2$  has a good behaviour.

In the limit  $u \rightarrow +\infty$  the dilaton behaves as

$$(\partial\varphi)^2 = \frac{81k^2}{(16 - 9k^2)^2} (\mu_1 - \mu_2)^2 \left( \frac{C_1}{2E_1} \right)^{\frac{16}{16-9k^2}} \left( \frac{C_2}{2E_2} \right)^{\frac{9k^2}{9k^2-16}} e^{\frac{2(16\mu_1-9k^2\mu_2)}{16-9k^2}u}. \quad (\text{B.7})$$

The divergence disappears for  $\mu_1 = \mu_2$  in the non-vacuum case.

## C Details of the non-vacuum RG

In this section we present some properties of our solutions on the plots. In Sect.5.3 we show that the RG functions  $X$  and  $Y$  as functions of  $\phi$  have pole at point  $f_s$ . Now at Fig. 31 we plot  $X$  and  $Y$  and their derivative as functions of  $u$ . At Fig. 31 we see that other quantities, namely,  $V$  and  $R = X^2 - Y - 1$  for all values of  $\alpha^1$  are finite at the jump point.

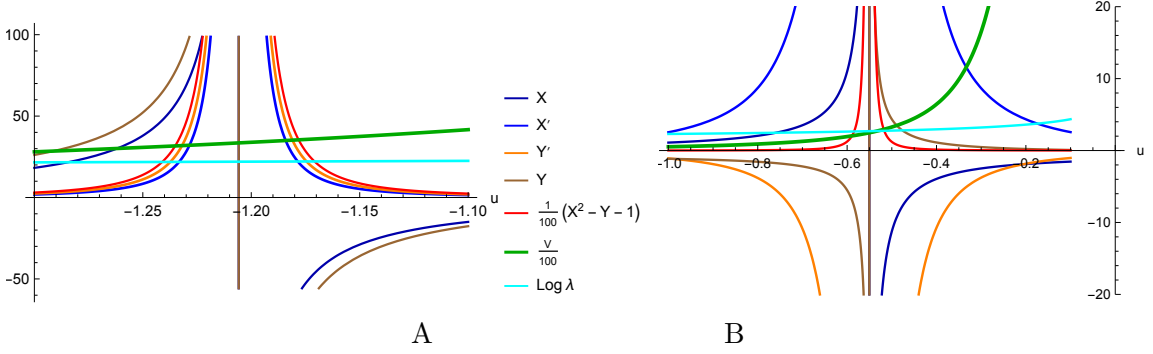


**Figure 31.** Details for the left solution. Typical behavior of  $X, X'_u, Y, Y'_u, X^2 - Y - 1, V, \phi$  near the jump point  $u = u_s, \phi(u_s) = f_s$  for positive  $\alpha^1$  A) and for negative  $\alpha^1$  B).

At Fig. 32 we show that intersection of RG flow with the critical line corresponds to the zero of the potential.

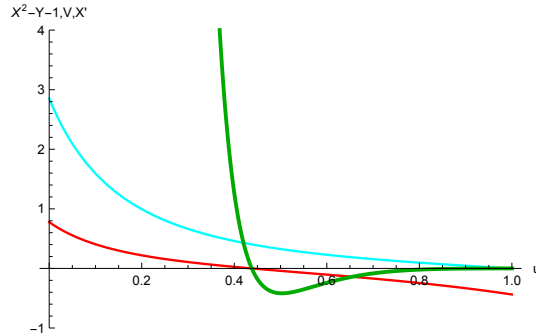


**Figure 32.** Details of the RG for the middle solution: Intersection of the critical line corresponds to the zero of the potential:  $X^2 - Y - 1$  – red line,  $V$ – green line,  $X'$  – cyan line.

From Fig. 33 we see that the form of the right flow (the flow on the right solution) does not depend on the values of  $u_{01}$  and  $u_{02}$  for  $u_{01} \neq u_{02}$ .

Fig. 34 shows that at large  $u \rightarrow +\infty$  the RG functions  $X$  and  $Y$  go to some fixed values at the critical line.

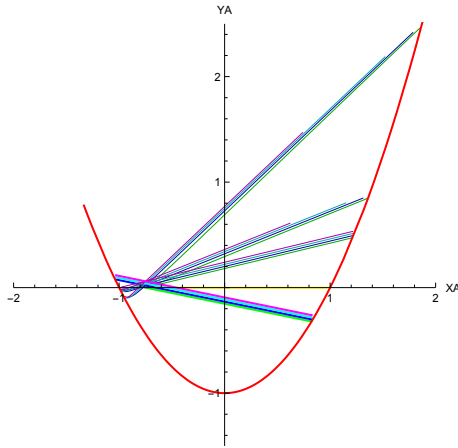


**Figure 33.** Details for the right solution, the same as at Fig.17 for different  $u_{02} = 1, 2, 3, 4$  with small shifts in  $Y$  to show that in fact there is no dependence on  $u_{02}$ .

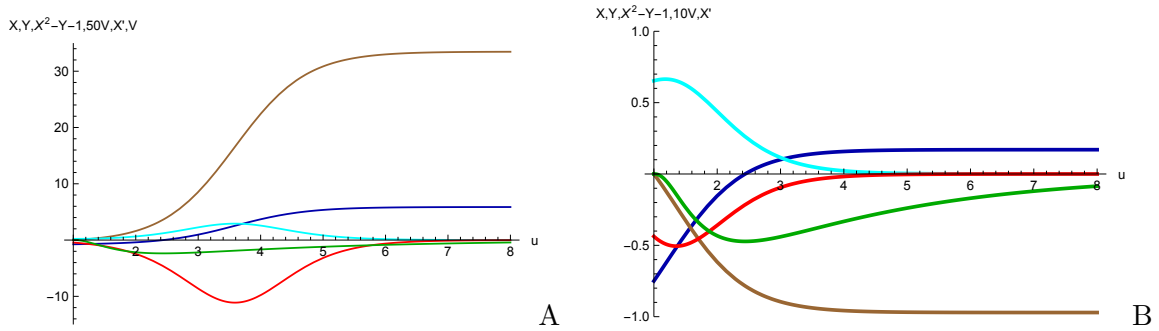


**Figure 34.** Details for the right solution: A)  $X, Y, X^2 - Y - 1, X'$  and  $V$  as function of  $u$  for negative  $\alpha^1$ ; B) the same as at A) for positive  $\alpha^1$ . Here  $X$  is the brown line,  $X^2 - Y - 1$  - red line,  $Y$  - blue line,  $V$  - green line,  $X'$  - cyan line

## References

- [1] J. de Boer, E. P. Verlinde and H. L. Verlinde, On the holographic renormalization group, *JHEP* **0008** (2000) 003; [[hep-th/9912012](#)].
- [2] I. Heemskerk and J. Polchinski, Holographic and Wilsonian Renormalization Groups, *JHEP* **1106** (2011) 031; [[arXiv:1010.1264](#)].
- [3] T. Faulkner, H. Liu and M. Rangamani, Integrating out geometry: Holographic Wilsonian RG and the membrane paradigm, *JHEP* **1108** (2011) 051; [[arXiv:1010.4036](#)].
- [4] S. S. Lee, Quantum Renormalization Group and Holography, *JHEP* **1401** (2014) 076; [[arXiv:1305.3908](#)].
- [5] E. Kiritsis, F. Nitti, L. S. Pimenta, Exotic RG flows from Holography, *Fortsch.Phys.* **65** (2017) 2, 1600120; [[arXiv:1611.05493](#)].
- [6] H.A. Chamblin and H.S. Reall, Dynamic Dilatonic Domain Walls, *Nucl.Phys.* **B 562** (1999) 133-157; [[hep-th/9903225](#)].
- [7] U. Gursoy, M. Jarvinen, G. Policastro, Late time behavior of non-conformal plasmas, *JHEP* **1601** (2016) 134 [[arXiv:1507.08628](#)].
- [8] P. Betzios, U. Gursoy, M. Jarvinen and G. Policastro, Quasi-normal modes of a strongly coupled non-conformal plasma and approach to criticality, [[arXiv:1708.02252](#)].
- [9] A. N. Leznov and M.V. Saveliev, Group theoretical methods for integration of nonlinear dynamical systems, Nauka, Moscow, 1985.
- [10] A. M. Perelomov, Integrable systems of Classical Mechanics and Lie Algebras, Nauka, Moscow, (1990).
- [11] U. Gursoy, E. Kiritsis, L. Mazzanti, F. Nitti, Holography and Thermodynamics of 5D Dilaton-gravity, *JHEP* **0905** (2009) 033; [[arXiv:0812.0792](#)].
- [12] B. Gouteraux, E. Kiritsis, Generalized holographic quantum criticality at finite density, *JHEP* **1112** (2011) 036; [[arXiv:1107.2116](#)].
- [13] D. Z. Freedman, S. S. Gubser, K. Pilch and N. P. Warner, Renormalization group flows from holography supersymmetry and a c-theorem, *Adv. Theor. Math. Phys.* **3**(1999) 363; [[hep-th/9904017](#)].
- [14] E. Kiritsis, W. Li and F. Nitti, Holographic RG flow and the Quantum Effective Action, *Fortsch. Phys.* **62** (2014) 389; [[arXiv:1401.0888](#)].
- [15] V.R. Gavrilo, V.D. Ivashchuk and V.N. Melnikov, Integrable pseudo-Euclidean Toda-like systems in multidimensional cosmology with multicomponent perfect fluid, *J. of Math. Phys.*, **36** (1995) 5829; [[hep-th/9407019](#)].
- [16] V.D. Ivashchuk, V.N. Melnikov and A.B. Selivanov, Cosmological solutions in multidimensional model with multiple exponential potential, *JHEP* **0309** (2003) 059; [[hep-th/0308113](#)].
- [17] A.A. Golubtsova and V.D. Ivashchuk, Exact solutions in gravity with a sigma-model source, *Gen.Rel.Grav.* **44** (2012), 2571-2594; [[arXiv:1204.0091](#)].